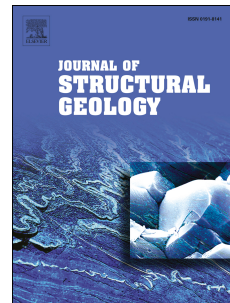


Journal Pre-proof

Evolution of the stress field near the Arava basin located along the Dead Sea Fault system as revealed by joint sets

Tsafrir Levi, Yoav Avni, Dov Bahat



PII: S0191-8141(19)30027-6

DOI: <https://doi.org/10.1016/j.jsg.2019.103876>

Reference: SG 103876

To appear in: *Journal of Structural Geology*

Received Date: 20 January 2019

Revised Date: 4 August 2019

Accepted Date: 21 August 2019

Please cite this article as: Levi, T., Avni, Y., Bahat, D., Evolution of the stress field near the Arava basin located along the Dead Sea Fault system as revealed by joint sets, *Journal of Structural Geology* (2019), doi: <https://doi.org/10.1016/j.jsg.2019.103876>.

This is a PDF file of an article that has undergone enhancements after acceptance, such as the addition of a cover page and metadata, and formatting for readability, but it is not yet the definitive version of record. This version will undergo additional copyediting, typesetting and review before it is published in its final form, but we are providing this version to give early visibility of the article. Please note that, during the production process, errors may be discovered which could affect the content, and all legal disclaimers that apply to the journal pertain.

© 2019 Published by Elsevier Ltd.

Evolution of the stress field near the Arava basin located along the Dead Sea Fault system as revealed by joint sets	1 2
Tsafrir Levi ¹ , Yoav Avni ¹ , Dov Bahat ²	3
1. Geological Survey of Israel, 30 Malkhe Israel St., Jerusalem 95501, Israel	4
2. Department of Geological and Environmental Sciences, Ben-Gurion University of the Negev, Beer-Sheva, Israel	5 6
	7
Abstract	8
To reveal the development of the stress field near the Arava basin located along the Dead Sea Fault system, we characterized joint sets that were exposed mainly in the Santonian and Eocene chalk rock outcropping in the study area.	9 10 11
In total, ~2600 strike orientations of single-layer joints (SLJ) and multilayer joints (MLJ) mirrored four main stress fields: 1) $\sigma H_{\text{NW}}(J1-326^\circ)$, 2) $\sigma H_{\text{NNW}}(J2-343^\circ)$, 3) $\sigma H_{\text{NNE}}(J3-033^\circ)$, and 4) $\sigma H_{\text{N}}(J4-360^\circ)$.	12 13 14
The results showed that the relatively lower values of the fracture spacing ratio (FSR) and their standard deviations in J1 implied that J1 was formed during the burial stage of the Eocene chalk formations. The inconsistency between the statistical parameters of the log-normal distributions of joint spacing and FSR raised doubt about the applicability of the "saturation joint density model" in our studied area.	15 16 17 18 19
The joint sets characteristics suggest that the regional σH_{NW} operated during the Eocene. During the Miocene, the regional stress field changed clockwise to σH_{NNW} , probably in association with the early stage of transform motion along the Dead Sea Fault. In the Pliocene-Pleistocene, the σH_{NNE} and σH_{N} local stress fields both operated and were accompanied by a tensional stress field that can be identified in the intensive normal faulting evolved along the western Arava basin margins.	20 21 22 23 24 25

1. Introduction	26
<i>1.1. Stress field along boundary faults</i>	27
The stress field next to plate tectonic faults (i.e., generally up to several km and more depending on the fault dimensions; see Rebai et al., 1992), such as the Dead Sea Fault (DSF) (Fig. 1), often deviates from the regional stress field (i.e., remote stress field) related to plate movements and plate tectonics (e.g., Garfunkel et al., 1981; Dewey et al., 1998; Gomez et al., 2006; Weinberger, 2014; Fossen, 2010; Guidi et al., 2013; Veloso et al., 2015). Hence, the local stress field may be quite variable with respect to orientation, while regional tectonic stress patterns may be found to be consistent over large areas (Rawnsley et al., 1992) where the plate boundary forces act in a single dominant direction (Heidbach et al., 2018).	36
Plate tectonic faults may be accompanied by belts of deep tectonic basins that develop during geological times (e.g., Okay et al., 1999; Garfunkel et al., 2014), such as the young Arava basin in the DSF (Avni et al., 2012). Determining the stress field near such basins and its geologic history is a key factor in understanding the associated tectonic and mechanical processes accompanying these structures. Despite the importance of determining the paleo-stress field and associating it with the development of tectonic basins, in most cases, it is difficult to distinguish between the effect of the remote and local stress fields, especially near major faults such as the DSF (e.g., Levi and Weinberger, 2011). This difficulty arises mainly because the local stress field is likely to be complex; in some locations close to the faults, meso-scale kinematic indicators are absent, and it is not always clear which structural characteristics determine the local stress field.	48
In this study, we characterized joint sets that are intensively exposed in the Arava basin, along the Dead Sea Fault system. Based on joint strike orientations measured from the	50

Santonian and Eocene chalk formations—i.e., joint characteristics—we show that the regional stress field changed in a new direction in the last stage of development of the Arava Basin, the Dead Sea fault system, and became localized. The study demonstrates how the analysis of joint sets can be used as a sensitive tool to identify complex stress fields close to a boundary fault. Therefore, it may prove helpful in recovering the paleo stress field to study deformation near boundary faults such as the development of depression basins. Beyond the tectonic aspects, this paper investigated joint spacing to expand our understanding of joint development in sedimentary layers.	51 52 53 54 55 56 57 58
The joint (opening-mode I fractures) develops in the plane perpendicular to the least compressive stress (σ_3) and parallel to σH_{\max} (the most compressive horizontal stress). Joints are one of the most sensitive markers of small strain or stress changes (Pollard et al., 1982; Rawnsley et al., 1992). Thus, they are sensitive indicators of paleo stress fields and can be used to infer the regional (scale of tens of kilometers) and local (i.e., scale of several kilometers generally in association with faults or folds) horizontal stress field (σH_{\max}) along with its spatial evolution (e.g., Engelder and Geiser, 1980; Holst and Foote, 1981; Engelder, 1982; Flexer et al., 1984; Hancock, 1985; Bevan and Hancock, 1986; Dyer, 1988; Bahat and Grossmann, 1988; Pollard and Aydin, 1988; Simón, 1989; Hancock and Engelder, 1989; Liotta, 1990; Hancock, 1991; Gross and Engelder, 1991; Laubach et al., 1998; Bahat, 1998a; Arlegui and Simóñ, 2001; Eyal et al., 2001; Chu et al., 2013; Tavani et al., 2015) and timing using fluid inclusions and temperature history proxies for timing (Laubach et al., 2009, 2016).	59 60 61 62 63 64 65 66 67 68 69 70 71
<i>1.2. Joint characteristics in sedimentary rocks</i>	72
To determine a stress field in association with tectonic events, the joint sets must be examined according to different criteria indicating the fracture conditions prevailing at the time of their development.	73 74 75

The relationship between joint height (H) and spacing (S) can be quantified by the fracture spacing ratio (FSR) and fracture spacing index (FSI). The FSR (Gross, 1993) is the bedding height (termed as "fractured layers"; Laubach et al., 2009) divided by the median joint spacing for an individual bed. The FSI is the slope of the regression line fitted to a plot of bedding height versus median joint spacing derived from scanline data (Narr and Suppe, 1991; Gross, 1993; Engelder et al., 1997; Ruf et al., 1998). The FSR and FSI are useful to document the joint intensity within individual and numerous layers (e.g., Jiang et al., 2016), respectively; therefore, they can be used to estimate strain magnitudes (Eyal et al., 2001).

Joint spacing distributions may reveal important aspects of the fracturing process, such as the degree of joint set development (Huang and Angelier, 1989; Narr and Suppe, 1991; Rives et al., 1992; Fischer, 1994; Becker and Gross 1996; Ruf et al., 1998; Rabinovitch and Bahat, 1999; Gillespie et al., 1999). Kurtosis is a measure of the peakedness or flatness of a frequency distribution relative to a normal (Gaussian) distribution, which, by definition, has zero Ku. When the bedding interfaces have a large effect on the joint growth (hereinafter, "single layer joint" (SLJ)), a range of fracture sizes can exist in such a fracture array ("bed-bound fractures"), but the maximum size is limited in one dimension to match the layer thickness (Hooker et al., 2013). When the fractures are not perfectly bed bound, the fractures may vertically cross the bedding interface boundaries ("unbound fractures") or may cross several bedding interfaces (hereafter, "multilayer joint" (MLJ)).

In many cases where the fractures develop in beddings far from the fault, the joint spacing is more or less even or random (Laubach et al., 2018). Areas of anomalously close fracture spacing (Laubach et al., 2018) may develop near faults (e.g., Becker

and Gross, 1995); these are usually termed joint and vein arrays (e.g., Delaney et al., 1986) or corridors (e.g., Belgrano et al., 2016) or swarms (Laubach et al., 1995).	100 101
The degree of clustering or irregular spacing (Laubach et al., 2018) in joint distribution can be analyzed using the relationship between the standard deviation of spacing (S_{stdv}) and mean joint spacing (Gillespie et al., 1999)—i.e., the coefficient of variation. If fractures are clustered, then $Cv < 1$; if they are anti-clustered (i.e., regularly spaced), then $Cv > 1$ (Gillespie et al., 1999).	102 103 104 105 106
Fracture surface morphology provides information about the stress and mechanisms involved in the development of a fracture (Bahat, 1979; Bahat, 1991; Bankwitz and Bankwitz, 1994; Bahat, 1999a; Weinberger, 1999, 2001). Generally, the FSM in rocks is divided into two main adjacent regions: the joint plane and fringe. The joint plane may be decorated with the critical flaw showing the origin, mirror plane, radial striae (plumes), concentric undulations (ripple marks with arrest lines), mist and hackle. The concentric undulations, radial striae and arrest lines may be associated with subcritical fracture velocity conditions, whereas the mist and hackle may to be associated with critical velocity (Bahat et al., 2012).	107 108 109 110 111 112 113 114 115
2. Geologic setting	116
<i>2.1. Study area</i>	117
The DSF system (e.g., Quennell, 1959; Freund et al., 1968; Garfunkel, 1981; Sneh and Weinberger, 2014) is an active tectonic element in the Middle East (e.g., Ben-Menahem et al., 1976; Salamon et al., 2003; Garfunkel et al., 2014) extending from the Red Sea in the south to Turkey in the north across almost 1,000 kilometers (Fig. 1). The left-lateral displacement along the transform plate boundary and vertical displacements along normal faults in the DSF system are probably the major source of the strain stored in the rocks along this structure, resulting in seismic activity and	118 119 120 121 122 123 124

internal deformation of the plates adjacent to DSF. The trace of the DSF along its southern segment in Sinai and Israel is characterized by a series of saddles and elongated <i>en echelon</i> tectonic sub basins forming depressions, extending over a stretch of 500 kilometers from the Gulf of Eilat (Aqaba) basin in the south and through the Arava Basin, Dead Sea Basin, Jordan and the Hula Basins in the north (Fig. 1).	125 126 127 128 129 130
2.2. Tectonic configuration	131
The Arava tectonic basin is 170 km long and 10-15 km wide and connects the Gulf of Eilat in the south and Dead Sea in the north. The Arava Basin is dissected by several major faults, forming a narrow fault zone that offsets a series of Pleistocene-Holocene alluvial fans, especially along its eastern part (Garfunkel et al., 1981; Ginat et al., 1998; Avni et al., 2000; Le Be' on et al., 2012; Garfunkel et al., 2014). According to the Seismic reflection survey by Frieslander (2000), the subsurface structure of the Arava Basin includes several buried Miocene grabens, accommodating sections of the Hazeva Formation of Early-Late Miocene age and Arava Formation of the Pliocene-Early Pleistocene age (Avni et al., 2001), indicating a long period of tectonic activity along the border faults of these structures. Based on GPS measurements, Masson et al., (2015) suggested that the current relative horizontal movement from Sinai to Arabia along the Arava fault varies while the velocity in its central part is 4.7 ± 0.7 mm/yr.	132 133 134 135 136 137 138 139 140 141 142 143 144
The current research focuses on the western margin of the central segment of the Arava Basin located between the Zofar and Paran settlements (Fig. 1). Several fault systems dissect the study area: the Zihor fault, whose directions are approximately north-south (Avni et al., 1994; Avni, 1998; Ginat, 1997; Karcz, 1997; Fig. 1b), and the Zenifim-Zihor-Baraq Fault line and Zhiha Fault, whose direction is north-	145 146 147 148 149

northeast and east-west Paran Fault (Sakal, 1998). The Paran Fault divides the study	150
area into two main regions: the northern region that includes Ramat Baraq and Har	151
Kippa and the southern region that includes Gva'ot Zehiha and Ramat Ovil (Fig. 1b).	152
The north-northeast Zenifim-Zihor-Baraq Fault is a normal fault line, and its	153
Pleistocene activity is dated to between 1 Ma and 400 Ka (Nuriel et al., 2011). Along	154
this tectonic line, there are several segments of subparallel normal faults that form a	155
series of eastward downfaulted blocks. The Ramat Baraq downfaulted block is located	156
east of the Baraq fault, while the Har Kippa uplifted block is located west of the fault.	157
The “Zihor Graben” is a long and narrow depression formed between the Zihor Fault	158
(to the west) and Zhiha Fault (to the east) (Avni, 1998). West of the Zihor Fault, the	159
uplifted block of Ramat Ovil develops, while east of the Zhiha Fault, the downfaulted	160
block of Gva'ot Zhiha develops. According to Avni et al. (2000), several Early	161
Pleistocene conglomerate units were displaced along this fault system, revealing the	162
recent rearrangements of the active fault system in the western margin of the Arava	163
Basin.	164
<i>2.3. Stratigraphy</i>	165
The rocks exposed in the study area belong to the Judea (Turonian-Coniacian), Mount	166
Scopus (Santonian-Paleocene), Avedat (Eocene), Tiberius (Miocene), and Dead Sea	167
(Pliocene-Pleistocene) groups (Fig. 1b, Table 1). Part of the exposed rocks in the	168
study area belongs to the Menuha consisting mainly of chalk and sometimes chert and	169
sandstone. Most of the exposed rocks in the study area belong to the Avedat Group,	170
whose ages range from the Early Eocene to Late Eocene, with a maximum thickness	171
reaching 314 m in the Nahal Paran section (Karcz, 1997). The Avedat Group (Braun,	172
1967) includes several formations consisting mainly of chalk and limestone, with	173
some chert layers. Benjamini (1979, 1984) divides the Avedat Group in the Arava	174

region into four formations: Mor, Paran, Matred and Kezi'ot. The Paran Formation	175
correlates with the Nizzana and Horsha formations known from the central Negev	176
region (Ben-Tor and Vroman, 1963).	177
The lower part of the Ramat Baraq section comprises the Mor Formation (Early	178
Eocene), which generally overlies the Taqiye Formation of the Paleocene-Early	179
Eocene age (Benjamini, 1984; Avni, 1998; Karcz, 1997). The Mor Formation consists	180
primarily of chalk layers with alternations of nodular chert layers. The Paran	181
Formation (Early-Middle Eocene) overlying the Mor Formation comprises chalk and	182
chalky limestone. The Har Kippa region mostly comprises the previously mentioned	183
Eocene section overlaid by the Matred Formation (Middle-Eocene) consisting of	184
alternations of limestone and indurated chalk (Korngreen, 1993; Karcz, 1997).	185
3. Methods	186
At least 10 primary joint orientations (strikes) were measured for each joint set in	187
each bed from the Menuha formation and Avedat group (Table 1). The measured	188
joints are vertical (above ~87°) and are formed in horizontal beds with a gentle dip of	189
up to ~2°. The observed secondary joints (i.e., orthogonal cross joints, etc.) that may	190
be associated with local stress rotation (Bai et al., 2002) were not included in this	191
study. Spacing data and joint lengths (on the map view) in the Mor formation along	192
each 1D scanline were collected. The joints in the study area are bed bound,	193
indicating that they are limited in one dimension to match the layer thickness, whereas	194
most of them developed from the bottom to the top of the layer boundaries (Fig.2a).	195
When several small joints whose heights were less than half of the layer thickness and	196
had abnormal densities (see "top-bound" joints in Hooker et al., 2013) were present,	197
they were not measured along the scan line. Spacing data were not taken adjacent to	198
the thoroughgoing fault or fracture zones to minimize local strain effects (Bahat,	199

1988; Becker and Gross, 1996). Joint spacing was calculated as the perpendicular 200
 distance between adjacent joints belonging to the same set. The bed thickness 201
 controlling the fracture height was measured in each scanline. Measurements of the 202
 heights of MLJ joints developed in the Paran formation (Fig. 2c) in the eastern area 203
 were carried out with a total station ($1 \pm \text{mm}$). The total station comprised a laser 204
 range meter to measure the distance from the station to the base of the joint and 205
 theodolite to measure the angle forms between the distance from the total station to 206
 the joint base and the distance from the total station to the top of the joint. The 207
 apertures of the MLJ joints, crosscuttings, abutting (e.g., Hancock, 1985; Dunne and 208
 North, 1990), fracture surface morphology (FSM) (Bahat, 1991 and references 209
 therein) and offsets of older joint sets by younger faults were used to determine the 210
 relative timing of joint-set formation within each bed. 211

4. Results

4.1. Joint sets

In total, 2,424 orientations of SLJ (Fig. 2a) in the Menuha, Mor, Paran and Zhiha 214
 Formations, outcropping in the entire study area and 222 orientations of MLJ (tens of 215
 meters) in the Paran Formation were measured (Fig. 2c). Based on the distribution of 216
 joint orientations and relative timing of the joint sets, four main sets are identified: 217
 (J1) $326^\circ \pm 3^\circ$, (J2) 343° , (J3) $360^\circ \pm 2^\circ$, and (J4) $033^\circ \pm 4^\circ$ (Figs. 3 and 4). 218

Based on various criteria (i.e., fracture abutments, cross-cutting relationships, and 219
 fractography), J1 is suggested to be the earliest set, whereas the J2, J4 and J3 sets 220
 developed one after the other sequentially (Figs. 2a,b, Supplementary data item #1). This 221
 conclusion is consistent with observations that show that J1 and J2 are formed only in the 222
 Menuha (Santonian-Early Campanian) and Mor-Matred (Early-Middle Eocene) 223

formations, whereas J3 and J4 are formed also in the younger Arava-Zhiha formations (Pliocene- Early Pleistocene).	224 225
J1 is observed in the Santonian-Early Campanian Menuha Formation, in the chalk layers of the Early Eocene Mor Formation and in the Paran and Matred Formations of Early to Middle Eocene age. This joint set is dominant in the study area (25% of all the analyzed joints): 39% of all the joints in the northern area and 23% of all the joints in the southern area.	226 227 228 229 230
J2 is observed in the Menuha Formation, in the chalk and chert layers of the Mor Formation and in the Paran and Matred formations. Occasionally, this set is also observed in the thin clay layers, appearing alternately between the chalk layers of the Mor Formation. J2 is dominant in the study area (35% of all the analyzed joints) but common in the northern (17% of all the joints) and southern study areas (51% of all the joints). Figure 3b shows two peaks in the distribution orientations of J2: 342° is dominant, and 349° is observed only at a few sites in Gva'ot Zhiha.	231 232 233 234 235 236 237
J3 is observed in the Menuha Formation, in the chalk and chert layers of the Mor Formation, and occasionally in the Arava Conglomerate and Zhiha Formation of the Early Pleistocene age. Occasionally, this set is also observed in the thin clay layers, appearing alternately between the chalk layers of the Mor Formation. J3 is observed (14% of all the joints) only in the eastern part of the northern area (4% of all the joints) and eastern part of the southern study area (12% of all the joints). In this set, 34 MLJs (005° ± 5°) with an aperture of 5 cm (in average) were documented in Ramat Baraq, in the eastern area (Fig 3e).	238 239 240 241 242 243 244 245
J4 is common in the chalk layers of the Mor Formation and the Paran Formation and occasionally observed in the Arava Conglomerate and Zhiha Formation. Occasionally,	246 247

this set is also observed in the thin clay layers, appearing alternately between the chalk layers of the Mor Formation. J4 is (19% of all of the joints) widespread in the eastern part of the northern area (40% of all the joints) as well as in the eastern part of the southern area (14% of all the joints) of the study. In this set, 182 MLJs ($032^\circ \pm 5^\circ$) with an aperture of 5 cm (in average) were documented in Ramat Baraq in the eastern area (Fig. 3e). The total number of joints of sets $280^\circ \pm 5^\circ$, $52^\circ \pm 4^\circ$ and $304^\circ \pm 4^\circ$ compared with the four main joint sets is relatively low (lower than 4% of all the joints).

Based on various criteria (i.e., fracture abutments, cross-cutting relationships, and fractography), J1 is suggested to be the earliest set, whereas the J2, J4 and J3 sets developed one after the other (Supplementary data item #1). This conclusion is consistent with the observations that J1 and J2 are formed only in the Menuha (Santonian-Early Campanian) and Mor-Matred (Early-Middle Eocene) formations, whereas J3 and J4 are also formed in the younger Arava-Zhiha formations (Pliocene- Early Pleistocene).

4.2. Joint spacing

From eleven outcrops in the chalky Mor Formation and four outcrops in the Menuha Formation (Ramat Oviv area), we measured 238 and 130 joint spacings of J1. The skewness and kurtosis suggest that all the spacing distributions are log normal type and positively skewed (Hooker and Katz, 2015) (Fig. 5). The kurtosis value in the chalk of the Mor Formation is higher (10.9) than that of the Menuha Formation (0.14) (Supplementary data item #2). The coefficient of variation value of the chalk of the Mor Formation (0.59) and the Menuha Formation (0.48) (Supplementary data item #2) showed that the joint spacing is close to a moderately even distribution.

The average FSR (i.e., bedding height divided by the median joint spacing for an individual bed) obtained from the eleven outcrops is 4.13, whereas the FSI is lower (3.56), with a relatively high correlation value ($R^2 = 0.94$) (Fig. 6a, Supplementary data

item #2). The ratios of the length to spacing (L/S) and height to length (H/L) obtained 273
from five outcrops are 4.44 and 0.89, respectively (Fig. 7; Supplementary data item #2). 274
From fourteen outcrops in the chalky Mor Formation, four outcrops in the nodular chert 275
layers of the Mor Formation and three outcrops of the Menuha Formation (Ramat Ovil 276
area), we measured 313, 109 and 134 joint spacings of J2, respectively. 277
Similar to J1, the skewness and kurtosis values indicate that all the spacing distributions 278
are log-normal type. The kurtosis value (7.2) from the chalk of the Mor Formation is 279
higher than those of the cherts of the Mor Formation (2.2) and Menuha Formation (1.77) 280
(Supplementary data item #2). 281
The coefficient of variation value of the chalk in the Mor Formation is almost similar 282
(0.56) to that in the chert of the Mor Formation (51%) and Menuha Formation (0.54) 283
(Supplementary data item #2). The FSRs (in average) of J2 calculated from nine outcrops 284
of the chalky Mor Formation and four chert layers of the Mor Formation are 6.6 ($R^2 =$ 285
0.76) and 1.4, respectively (Fig. 6b, Supplementary data item #2). The L/S and H/L ratios 286
obtained from 3 outcrops are 20 and 0.39, respectively (Fig. 7, Supplementary data item 287
#2). 288
From twenty-five outcrops in the Mor Formation and 12 outcrops in the Paran 289
Formation, we measured 469 spacings of J3 (SL) and 161 spacings of J3 (ML), 290
respectively (Fig. 8). The kurtosis of the SLJ in the Mor Formation (11.84) is similar to 291
the MLJ in the Paran Formation (11.2), whereas the coefficient of variation value of the 292
MLJ (0.77) is higher than that of the SL (0.55). 293
The FSRs (average) of J3 (SLJ) calculated from twenty-five outcrops of the Mor 294
Formation and 12 outcrops of the Paran Formation (MLJ) are 4.1 ($R^2 = 0.63$) and 6.3, 295
respectively (Fig. 6c). The L/S and H/L ratios of the SL obtained from 3 outcrops of the 296
Mor Formation are 0.3 and 1.02, respectively (Fig. 7). From four outcrops in the Mor 297

Formation, two chert layers in the Mor Formation and three outcrops in the Menuha	298
Formation, we measured 52 spacings of J4 (SL), 29 spacings of J4 (SL) and 245 spacings	299
of J4. From four outcrops in the Paran Formation, sixty-one spacings of J4 (MLJ) were	300
also measured (Fig. 8).	301
The kurtosis values of SLJ obtained from the chalky Mor Formation and Menuha	302
Formation are 0.14 and 10.4, respectively (Supplementary data item #2), whereas the	303
coefficient of variation values of the SLJ are 0.48 and 0.93, respectively.	304
The kurtosis and coefficient of variation values of the MLJ in the Paran Formation are	305
and 0.55, respectively. The FSRs (average) of SLJ calculated from the chalky Mor	306
Formation (Supplementary data item #2) and chert layers of the Mor Formation are 7.4	307
and 1.33, respectively. The FSR (average) of MLJ from the Paran Formation is 4.8.	308
<i>4.3. Fracture Surface Morphology (FSM)</i>	309
In many cases, the shape of the parent joint near the nucleation area on the surface of the	310
joint sets was circular and, in several cases, elliptical (Fig. 9). Elliptical cyclical	311
undulations in the mirror plane parallel to the horizontal axis (rib markings) are very	312
common, indicating horizontal propagation parallel to σ_1 and that local (tens of cm)	313
mixed stresses (modes I + II) were imposed on the joint front. The distance from the	314
nucleation area is not constant. In several cases, radial plumes and, alternately, plumes are	315
identified on the surfaces of the joint sets, indicating that a local mixed stress (mode I +	316
III) was also imposed on the joint surface as well. In those cases, the plumes generally	317
crosscut the undulations orthogonally and emerged from the parent joint by creating an <i>en</i>	318
<i>echelon</i> crack. Generally, the sense of segment overlapping is clockwise.	319
The FSMs of the J2, J3, and J4 sets are observed in the chert layers of the Mor Formation	320
(Fig. 9b). Generally, the FSMs of the J2, J3 and J4 sets are similar to those of J1, except	321
for a given representative FSM, showing that the joint nucleation formed on chert	322

nodules is found within the chalk layers in the Mor Formation (Fig. 9c). These	323
observations indicate that the development of the J2, J3, and J4 sets occurred after the	324
consolidation of the chert and chalk layers.	325
In most of the MLJ, the surfaces are smooth (Fig. 9f), indicating that local tensional stress	326
was imposed on the joint surface (Bahat, 1991). In cases where the FSM could be	327
identified, the mirror is well developed, with a radius of 20-30 m. In cases where rib	328
markings could be observed, they are usually large (length of the perimeter 10-15 m) and	329
propagated horizontally or downwards.	330
5. Discussion	331
<i>5.1. General</i>	332
The four main joint sets in the present study, J1, J2, J3 and J4, are distinguished by their	333
orientations, abutting relationships and characteristics; they are also identified in	334
different zones of the study area and rock types (Figs. 3,4). Therefore, each of the joint	335
sets represents the stress field σ_H (i.e., maximum horizontal compressive stress), operated	336
at the time of its development in the Arava basin, near the DSF system.	337
Single-layer joint (SLJ) or bed-bound fractures can form in different geologic settings	338
such as burial, tectonic and uplift settings (Engelder, 1985, Bahat, 1988b). Under	339
certain conditions, such as pure tensional stress associated with geological uplift	340
settings (Bahat, 1988b) or under high stress magnitudes (Becker and Gross 1996), the	341
multilayer joints (MLJs) may cross several bedding interfaces. Considering this	342
characterization, the study findings show that J1 and J2 have only SLJ whereas J3 and	343
J4 also have MLJ, suggesting that the latter two joint sets have developed under	344
different geological settings.	345
	346
	347
	348

<i>5.2. Joint characteristics</i>	349
<i>5.2.1. FSRs, FSMs and field observations</i>	350
Figures 6 and 10 show the FSR values of the joint sets and their standard deviations,	351
respectively. The average FSR value (4.1) and FSI value (3.9) of J1 are very close (Fig.	352
7a) compared with those values in J2 (FSR=6.1; FSI=6.6) and J3 (FSR=4.1; FSI=3.2)	353
(Figs. 6b, c and Supplementary data item #2). Additionally, the FSRs of J1 and their	354
standard deviations are lower than those in the other three sets.	355
Field observations indicated that J1 is not formed in the chert layers of the Mor Formation	356
while J2, J3 and J4 are also observed in these layers (Figs. 9b, c). These observations	357
suggest that J1 developed during the burial stage of the chalk layer (Bahat, 1988b),	358
whereas J2, J3 and J4 developed after the consolidation of the chalk and nodular chert	359
layers.	360
Under burial conditions, it is very likely that each chalk layer was fractured in an	361
autonomic manner (Bahat, 1991, pp. 241, 258), whereby all the strain acting along the	362
layers was only accompanied by fracturing (see below).	363
Field observations indicated that, in few cases, several joints of the J2, J3 and J4 sets also	364
formed in the bedding planes built of the thin clay layers appearing alternately between	365
the chalk layers of the Mor Formation. These observations suggested that the layer	366
thickness is the main factor controlling the jointing spacing. However, opening and	367
shearing along interfaces under a low overburden (see "moderate" to "weak" interfaces	368
in Cooke and Underwood, 2001) can also occur. Under such conditions, the FSR values	369
are expected to be more scattered as obtained in the J2, J3 and J4 sets (Fig. 6c).	370
<i>5.2.2. Joint spacing "saturation"</i>	371
The range of the FSR values (1.33-7.4) is higher than the proposed threshold "saturation"	372
level (~1.5). Higher values of FSR above the "saturation" level were reported by Becker	373

and Gross (1996) and Eyal et al. (2001), raising the question of whether a saturation threshold of joint density existed in our studied area (Rabinovitch et al., 1999; Rabinovitch et al., 2012). Sagy and Reches (2006) based on field measurements in the western margins of the Dead Sea basin and an experimental observations suggested that fractures can produce tightly spaced patterns during dynamic propagation. Tan et al., (2014) showed that the range of the joint saturation ratio's (JSR) range between 4.09 and 40.09% corresponded with the FSI values ranging from 0.15 to 1.34. Although there is no need to have a good correlation between these two parameters, it can be assumed that the range of the FSRs of the present study may correspond to the range of JSRs higher than 4.09 to 40.09%. The FSM indicate that all the joint sets were not evolved during a relatively fast fracture velocity (Weinberger and Bahat, 2008). The statistical parameters of the joint spacing distributions show that all are log normal types, positively skewed, whereas the range of the CVs (0.48-0.93) implies that most of the joint spacing have medium clustering arrangement. Rives et al. (1992) and Wu and Pollard (1995) suggested, based on laboratory experiments, that the higher the degree of strain in a rock is, the higher the spacing density gradually becomes and, accordingly, the distribution tends to be more “normal” up to a stage in which the density of spacings reaches saturation. In accordance with these observations, Becker and Gross (1996) showed that the average of the joint spacings was decreased in the vicinity of the faults, whereby the Ku value increased accordingly. Against this, Ruf et al. (1998) showed that differences in the Ku values could be associated with differences in the isotropic degree of rocks. They suggested that high values of Ku could indicate that the rock was more anisotropic. Additionally, Huang and

Angelier (1989) suggested that differences in the spacing distributions could be associated 398
 with the lithification degree of the rock. 399

The present study shows that it is not possible to attribute all the spacing distributions to 400
 one general mechanical model mentioned above. For example, despite the difference in 401
 FSR between J1 (4.1) and J2 (6.6) (Fig. 6), the skewness and CVs of J1 ($sk=2.24$; 402
 $Cv=0.59$) and J2 ($sk=1.9$; $Cv=0.56$) (Supplementary data item #2) are almost similar, 403
 indicating that although both joint sets are characterized by a similar joint spacing 404
 distribution and clustering pattern, they are not characterized by the same FSR. 405

The difference in Ku could be related to the isotropic degree of the rock. This possibility 406
 may be considered given that the Ku values of J1 (10.9) and J2 (6.6) in the Mor 407
 Formation are much higher than those obtained in the Menuha Formation (0.14 and 1.77, 408
 respectively; Supplementary data item #2), while the Ku values in J4 are higher in the 409
 Menuha Formation (10.4) than in the Mor Formation (-0.14). Additionally, as shown in 410
 Figure 10, joint sets with relatively high FSR values also have high standard deviation 411
 values, indicating that the spacing distributions of those joint sets are not “normal”, as 412
 expected by Rives et al. (1992). 413

In the fractured layer, the crack-driving tensile stress decreases adjacent to the existing 414
 fracture in a region called the “stress shadow” or tension relief zone. Therefore, no 415
 new fractures form within this zone. Considering the commonly observed 416
 proportionality of joint spacing to layer thickness (e.g., Gross et al., 1995), the rock 417
 layers became saturated with joints (e.g., Becker and Gross, 1995). However, the 418
 validity of saturation is debatable because field observations (e.g., Eyal et al., 2001) 419
 suggest that localized strains can lead to high joint densities beyond the proposed 420
 “saturation” levels. 421

One possible explanation for the discrepancy between the high FSR values and those of the suggested models is that, during the sequential infilling process (Bai and Pollard, 2000) (i.e., new joints forming between two neighboring joints) and fracture opening, the early-generation joints were filled-cemented by fluid (Engelder and Lacazette., 1990 and referenced therein). Thus, the tension relief near the early fracture is lessened (Hooker and Katz, 2015) or relaxed (Olson et al. 2009), and the fracture spacing is decreased, resulting in FSRs higher than the expected theoretical value. Observations made in the study area show that some of the joints are filled-cemented by fluid mainly in the Menuha Formation, somewhat explaining the high FSRs. Another possible explanation is that J2, J3 and J4 were formed close to the surface where high stresses were imposed on the beds in an unconfined setting with a low overburden. These proposals should be elaborated upon in future works.

5.3. Stress fields near the Arava Basin

Mode I fracture sets (e.g., joints and veins) may form over a broad area of the continent (e.g., Arlegui and Simón, 2001; Laubach et al. 1998) under regional stress. On the other hand, these fracture sets may form in specific localities usually associated with major structures located nearby. Considering this common appearance, the findings of the present study indicate that J1 and J2 are regional sets (i.e., joint sets that reflect the regional stress field), while the J3 and J4 sets are local sets according to the following arguments: 1) J1 (25% of all the joints) and J2 (35% of all the joints) are observed throughout the entire area, while J3 (less than 20%) and J4 (less than 20%) are formed mostly in the eastern study area, parallel to younger NNE-SW Baraq and Zihor normal faults (Fig. 11) that are also located in the eastern study area; 2) in accordance with the relative timing among joint sets (section 4.1;Supplementary data item#1), it is suggested that J3 and J4 are the youngest sets, strengthening the affinity between J3 and

J4 to the local young normal faulting; 3) MLJ may form in association with uplift	447
settings (Bahat, 1988b), and normal faulting are documented only in the J3 and J4 sets,	448
outcropping in the eastern part of the study area (Fig. 12); 4) the outcrops of J4 are	449
arranged along north-south lines, implying the association with local E-W tension; and 5)	450
J1 and J2 are widely documented in the Negev and are reported in other places (tens to	451
hundreds of km from the study area) in the Israel region (e.g., Bahat and Grossman, 1988;	452
Eyal, 1996). These arguments strongly suggested that during the development of J3 and	453
J4, the stress field deviated from regional to local in the area adjacent to the Arava Basin	454
up to several kilometers to the west.	455
<i>5.4. Stress field associated with tectonic processes near the Arava Basin</i>	456
<i>5.4.1. Regional stress fields</i>	457
According to the study findings (see 5.2.1), and based on previous studies (see below), it	458
appears that σH_{NW} (326°) operated since the Early Eocene and probably continued into the	459
Middle Eocene or even up to the Late Oligocene-Early Miocene.	460
The σH_{NW} is widely documented in Negev and other places throughout Israel.	461
Based on SLJ measurements, Bahat and Grossman, (1988) as well as Bahat, (1998b)	462
suggested that σH_{NW} was regional-continental and operated since the Early Eocene and	463
probably continued into the Middle Eocene. Similar to the present findings, Bahat (1999)	464
showed that the SLJ- 328° formed in the Lower Eocene chalks near Beer Sheva do not	465
cross the chert beds, implying that this joint set developed during the burial history of	466
the rock. Sakal (1998), based on joint measurements, found early activity of σH_{NW} in the	467
Paran zone region. Karez (1997) and Avni (1998), based on observations made along the	468
Baraq and Zihor-Zehiha Fault, suggested that tectonic activity that began in the Early-	469
middle Eocene was accompanied by the activity of reverse faults whose general	470
orientation was north-northeast. Karcz (1997), based on mapping the Ramat Barak area,	471

suggested that, during the Eocene, the Baraq fault acted as a reverse fault but he did not 472
 know to what stress field to attribute this tectonic activity. Ginat (1997) suggested that the 473
 NW normal faults located near the Zenifim fold formed after the development of the 474
 Syrian Arc folds, mainly during the late Cretaceous (Eyal, 1996 and references therein). It 475
 is very likely that the regional σH_{NW} is the appropriate stress field that could explain the 476
 north-northeast oriented reverse fault and development of structures (i.e., fractures and 477
 normal faults) with a general orientation of northwest that are widespread in the Negev 478
 and Sinai subplate (Avni et al., 2012) and may also explain the formation of NE-SW folds 479
 in the Levant Basin during the Late Eocene-Oligocene (Sagy et al., 2018). Furthermore, 480
 based on Avni et al., (2012), it is likely that σH_{NW} is related to tectonic activity in the 481
 Eocene responsible for the deposition of marine debris flows and intraformational clastic 482
 units that occurred at that time (named the Temed clastics in Avni et al., 2012 and 483
 references therein). 484

In the Early Oligocene, this stress field may have promoted the development of grabens 485
 and their related conglomerates (named the Mahatardi Conglomerates in Avni et al., 2012 486
 and references therein), concentrated mainly along NW pre-existing faults. Because many 487
 of the dike swarms are oriented NW, parallel to the Red Sea and widespread in the Sinai 488
 subplate and Arabian Plate (Eyal et al., 1981; Avni et al., 2012), we speculated that the 489
 pre-existing fractures that formed by the σH_{NW} promoted the penetration of dikes during 490
 the Late Oligocene-Early Miocene. 491

During the Early or Late Early Miocene, the regional stress field in the study area was 492
 $\sigma H_{NNW(343^\circ)}$ (Eyal and Reches, 1983; Hatzor and Reches, 1990; Baer and Segev, 1996) 493
 and was changed clockwise in the direction from σH_{NW} by $\sim 17^\circ$, suggesting that the 494
 location of the plate tectonic collisions, Europe-Arabia and Asia, and its dominance in 495
 influencing the regional stress changed during this time span (Heidbach et al., 2018). 496

Therefore, these findings may support the "stress rotation" model (e.g., Bahat, 1999b; Voznesensky et al., 2002) which considers that during a certain time span, the regional stress rotated clockwise. 497
498
499

The high FSR values (average, 6.6) of J2 that are statistically distinct from the FSR values of J2 (Fig. 10) indicate that, during the activity of, σH_{NNW} , the joints developed at denser spacing compared with J1. The anomaly of this joint spacing density (i.e., high FSR) was also documented by Eyal et al. (2001) who measured the joint set in the Neqarot syncline of south-central Israel and showed that the joint set (NNW-SSE) is characterized by high FSR values (~0.8-7.4). 500
501
502
503
504
505

The σH_{NNW} may be associated with the left-lateral motion formed along the Arava segment of the DSF system (Eyal and Reches, 1983; Eyal, 1996), whose general direction is North-Northeast (Bartov, 1994; Eyal and Reches, 1983; Eyal, 1996). The activity of the σH_{NNW} in the study could have begun during the Early or Late Early Miocene. If the σH_{NNW} began to operate during this Early Miocene, J2 may predate (e.g., Peacock., 2001 and references therein) the left-lateral occurring mainly during the Late-Early Miocene (Quennell, 1959; Freund et al., 1968; Bartov et al., 1980; Eyal et al., 1981; Garfunkel, 1981; Joffe and Garfunkel, 1987; Livnat and Flexer, 1987; Eyal, 1996; Sneh, 1996; Nuriel et al., 2017). During the Early-Late Miocene, at least three tectonic events were accompanied by uplift and truncation (Calvo and Bartov, 2001; Avni et al., 2000, 2012). 506
507
508
509
510
511
512
513
514
515

If the σH_{NNW} began to operate in the study area during these tectonic events, then the σH_{NNW} in the study area is associated directly with the shear movement along the Arava segment. 516
517
518

5.4.2. Local stress fields associated with tensional component 519

According to the study findings (see section 5.3), it appears that the regional stress (σH_{NNW}) was changed in the study area to two local stresses: $\sigma H_{N(033^\circ)}$ and $\sigma H_{N(360^\circ)}$, which 520
521

were operated sequentially. The high MLJ and their large apertures that were 522
 documented in J3 and J4 imply that both $\sigma H_{N(033^\circ)}$ and $\sigma H_{N(360^\circ)}$ were also accompanied by 523
 tensional stresses. Although the R^2 of the FSRs in each joint set is low, the common 524
 regression line of the two joint sets has relatively high R^2 value (0.66), suggesting that 525
 both joint sets were apparently developed under similar geological conditions. 526
 J3 and J4 are formed mostly in the eastern study area, parallel to younger (Pliocene-early 527
 Pleistocene) NNE-SW Baraq and Zihor normal faults, suggesting that they are relatively 528
 younger joint sets and that they have an affinity to the eastern part of the study area. 529

The local σH_N was also documented in other regions in different studies, such as in the 530
 Timna region (Mart and Horowitz., 1981), the Wadi Araba segment region (Eldeen et al., 531
 2000), the Reches Menucha Anticline (Voznesensky et al., 2002), the Rosh Pina (Issachar 532
 et al., 2015) and the Golan Heights area (Issachar et al., 2018). 533

The tensional stress component, as identified by the high MLJ in the Arava Basin, 534
 occurs in accordance with the observations reported by Garfunkel (1981) and Joffe 535
 and Garfunkel (1987), who suggested that since 5-6 m.y. ago, the stress field near the 536
 DSF was also accompanied by a tensional stress (E-W) component. It is very likely 537
 that this stress field component was associated with the grabenization process and 538
 uplift that operated along the north-northeast faults (Baraq, Zihor and Zhiha faults) 539
 after the deposition of the Early Pleistocene Arava and Zhiha Formations (Avni, 1998; 540
 Ginat, 1997). 541

Based on the above, J3 and J4 and their associated MLJ were linked to the tectonic 542
 phase that occurred in the western margins of the Arava rift during the Pliocene-early 543
 Pleistocene. This tectonic activity operated mostly during the Early Pleistocene along 544
 the pre-existing north-northeastern faults that were combined with a general tilt 545
 toward the Arava tectonic depression. This activity was accompanied by local 546

tensional stress (Meirov et al., 2007) that activated normal faults, downfaulted the	547
Arava depression, uplifted the western margins of the Arava Basin (e.g., Har Kippa)	548
and reversed the flow of the streams that had previously flowed westward (Avni,	549
1998; Avni et al., 2000).	550
<i>5.5. Development of the local stress fields</i>	551
Several mechanisms could explain the deviation of the remote strain fields close to the	552
DSF. Stress perturbations (i.e., dislocation stress fields) are expected in regions that are	553
close to seismically active faults (e.g., Trepmann and Stöckhert, 2001). Coseismic slip	554
can deflect the stress field surrounding a fault (e.g., Yukutake et al., 2010; Ma and	555
Andrews, 2010), and such stress perturbations were only partially recovered during post-	556
seismic activity (e.g., Nüchter and Ellis, 2011). The effects of fault strength (Garfunkel,	557
1981; Zoback et al., 1987; "weakening of fault"), stress buildup at fault edges, stress	558
partitioning along strike-slip faults (Weinberger et al., 2009), and fault geometry (e.g.,	559
Saucier et al., 1992) may also explain the reorientation of a regional stress field near	560
major faults.	561
Certainly, it is difficult to determine which of the above mechanisms is associated with	562
the local stress fields σH_{NNE} and σH_N near the Arava tectonic Basin. However, based on	563
the FSM, all the joint sets developed under sub critical conditions, indicating that they	564
were not evolved during a relatively fast fracture velocity (Weinberger and Bahat, 2008)	565
and local dynamic stress fields that developed near the rupture. Moreover, assuming that	566
the local joint sets were formed directly by the fault process, under such conditions, we	567
would expect the FSR of the local joint sets to be significantly higher than that of the	568
regional ones (Flinn, 1977) because the density of the joints (i.e., strain magnitude) is	569
higher adjacent to the fault (Mitchell and Faulkner, 2009). However, the results of our	570
study show that the FSRs of the local joint sets are relatively lower than or similar to the	571

FSRs of the regional joint sets (Fig. 7). Therefore, it does not seem likely that the young 572
local stress fields were formed directly by the fault process. 573

Stress rotation on a larger scale was proposed for the San Andreas fault in central 574
California (Zoback et al., 1987) and was found by Hatzor and Reches (1990) in the 575
Gilboa region. Garfunkel (1981) suggested that the directions of the principal stress 576
adjacent to the DSF were deflected toward the fault trace. He drew trajectories of 577
maximum compression that were subparallel to the "weak fault" traces (i.e., the fault that 578
reduces the shear stress along its planes) next to extensional areas (i.e., pull-apart basins, 579
such as the Arava tectonic depression) and orthogonal to the fault traces next to 580
contractional areas along the DSF. 581

The Pliocene-early Pleistocene local tensional stress field that was found in the Arava 582
tectonic Basin probably also operated (Garfunkel, 1981; Joffe and Garfunkel, 1987; 583
Lunina et al., 2005; Garfunkel et al., 2014 and references therein) in other tectonic 584
structures arranged along the DSF system (Sneh, 1996; Lunina et al., 2005; Mart et al., 585
2005). Based on structural measurements and analyses of the magnetic fabrics of 586
carbonated rocks, Weinberger et al. (2009) and Levi and Weinberger (2011) suggested 587
that a local W-E maximum shortening was dominant during the Pleistocene in the 588
Metulla block near the DSF, located approximately 400 km to the north of the study area. 589
Approximately 20 km further south of Metulla, analyses of magnetic fabrics indicated 590
that, near the Hula basin (Issachar et al., 2015) and further southward in the Arava basin 591
(Issachar et al., 2018), the stress field accommodated dominant E-W transtension during 592
the Pleistocene. 593

Evidence for early-mid Pleistocene tectonic activity is found in a series of basins 594
along the DSF. In the southern sector of the DSF from the Dead Sea basin southward, 595
a major tectonic phase, which started in the early Pleistocene, is marked by an 596

accelerated uplift of the DSF shoulders and subsidence of the basins along its axis (ten Brink and Ben-Avraham, 1989). In the central Dead Sea basin, rapid subsidence from the early Pleistocene is associated with accumulation of 4 km of sediments (Al-Zoubi and ten Brink, 2001). In the northern edge of the Dead Sea, subsidence of the Kalia and Jericho basins occurred probably throughout the Pleistocene. Further northward, a rapid subsidence of the Sea of Galilee basin is attributed to major geometrical reorganization of the DSF in the region started since ~1 ma (Hurwitz et al., 2002).

North of the Sea of Galilee a new phase of subsidence occurred in Hula basin during the mid-Pleistocene (Schattner and Weinberger, 2008).

Focal mechanisms and stress inversions along the southern segment of the DSF show that the dominant left-lateral motion is accompanied by an extensional component, normal to the trace of the DSF (e.g., Salamon et al., 2003; Hofstetter et al., 2007; Palano et al., 2013). Additionally, the world stress map shows (Heidbach et al., 2018) that in the southern part of the DSF, the stress regime comprises compressive and extensive stress components. Although it should be noted that measurements of GPS data along the Sinai and Arabian plates (e.g., Wdowinski et al., 2004; Al-Tarazi et al., 2011; Sadeh et al., 2012; Masson et al., 2015; Hamiel et al., 2016) do not clearly reflect the extensional component as verified in the present study and by analysis of the seismological data sets along the southern segment of the DSF.

Based on the aforementioned discussion, it is suggested that the local stress fields σH_{NNE} and σH_N were formed by the deflection of the remote stress field that may be compatible with the "weakness" of the DSF in southern Israel. Additionally, the development of the tensional stress field in the Arava Valley manifests the tectonic processes that changed mainly during the Early Pleistocene in basins along the DSF. In the future, a thorough study should be conducted along the Arava segment of the

Dead Sea fault to shed light on the development of σH_{NNE} and its association with the DSF system.	622
	623
6. Conclusions	624
A total of ~2400 joint strike orientations of SL and ~200 of ML joints measured near the Arava Tectonic Basin mirrored four main stress fields: 1) σH_{NW} (J1-326°), 2) σH_{NNW} (J2-343°), 3) σH_{NNE} (J3-033°), and 4) σH_{N} (J4-360°).	625
	626
	627
Analysis of the distribution of the joint spacings in different rocks shows that all are the log normal type, whereas most of the joint spacing have a medium clustering arrangement. In the past, several studies have suggested that rock layers become saturated at a certain level with joints. However, the present study shows, similar to other fieldwork, that no discrepancy exists between the statistical parameters of the spacing distributions and high FSRs that are beyond the proposed saturation level.	628
	629
	630
	631
	632
	633
Therefore, it is not clear how much the saturation of the joint density model is applicable in the study area.	634
	635
FSRs with relatively high correlation values ($R = 0.94$) and their standard deviations in J1 are lower than the rest of the joint sets. This implies that the development of J1 occurred during the burial stage the Mor Formation's chalk layers.	636
	637
	638
Based on the findings of the present study and the above discussion, σH_{NW} was likely regional and operated in the entire region during the Eocene.	639
	640
During the Early or Late Early Miocene, the stress field changed clockwise to σH_{NNW} , supporting the clockwise regional "stress rotation" model during this time span. This new stress field, which is manifested by a relatively denser joint set, may predate the strike-slip movement along the Dead Sea fault and later on during the Miocene, the DSF accommodated a left-lateral motion.	641
	642
	643
	644
	645

During the Pliocene-Pleistocene, the σH_{NNE} and σH_N local stress fields operated, and they were both accompanied by a tensional stress field evolved with intensive normal faulting (i.e., uplift settings) along the western Arava basin margins.	648
It is possible that the local stress field σH_N parallel to the DSF indicates that the western border faults of the Arava Basin are “weak”, explaining the relatively low number of earthquakes reported in the area (Garfunkel et al., 2014 and references therein), whereby the accompanied tensional stress field manifests the regional tectonic processes that deviated in the course of the young activity of the DSF system.	649
	650
	651
	652
	653
	654
Figure captions	655
Figure 1. a) Plate tectonic configuration of the study area (inset). The main faults of the DSF system are schematically marked (modified after Sneh and Weinberger, 2014) on the digital shaded relief map of Israel (Hall and Calvo, 2005). The fault trace at the surface and fault trace based on subsurface data are marked by black and dashed lines, respectively. b) Geological map of the Dead Sea Fault (DSF) in the study area (after Sneh et al., 1998). The names of the faults are marked. Circles mark the main study areas.	656
	657
	658
	659
	660
	661
	662
Figure 2. a) J2 observed in the Mor Formation (lower Eocene) and b) Arave Formation (Pliocene) adjacent to the Mor Formation outcrop. In this formation J2 is not observed. c) Multilayer joint set of J4 (see figure 3) observed in the Paran formation in the eastern part of the study area. d) abutting relationships between primary joint sets (J2) and secondray joints set (i.e., orthogonal cross joints). I and II mark two generation of J2. e) abutting relationships between J2 and J3 implies that J2 is the older joint set and f) J3 observed in Zhiha Formation.	663
	664
	665
	666
	667
	668
	669

Figure 3. Joint direction (strike) distribution of the northern area: a) all the joint directions with a moving average curve; b) Rose diagram of all the joint directions; c) joint directions from Har Kippa; and c) joint directions from Ramat Baraq. The main joint sets are marked above the distributions; and d) Rose diagram of the multilayer joint sets.	670 671 672 673 674
Figure 4. Joint direction (strike) distribution of the southern area: a) all the joint directions with a moving average curve; b) Rose diagram of all the joint directions; c) joint directions from Ramat Ovil; and d) joint directions from Gva'ot Zehiha. The main joint sets are marked above the distributions. Joint set distributions (%) are inserted in each histogram.	675 676 677 678 679
Figure 5. An example of normalized joint spacing distribution of J1 with the statistical parameters: a) joint spacing measured from the Mor Formation and b) joint spacing measured from the Menuha Formation.	680 681 682
Figure 6. FSR plots according to the joint sets: a) J1, b) J2 and c) J3.	683
Figure 7. L/S versus FSI plot of joint sets J1, J2 and J3, where J1 outcrops are marked by blue-filled diamonds, J2 outcrops are marked by red-filled squares and J3 outcrops are marked by purple-filled circles.	684 685 686
Figure 8. FSR plot of the multilayer joints of J3 and J4.	687
Figure 9. a) Circular undulations of J1, Mor Formation; b) undulations of J2 formed in the chert layer, Mor Formation; c) circular undulations of J2 formed around the nucleation area made by the nodular chert, Mor Formation; d) elliptical rib markings of J2 oriented 342° with red mineralization of vein-fill material; e) two single layer joints of J3 with elliptical rib markings, indicating horizontal propagation parallel to σ_1 ; and f) the smooth surface of J3 indicates that a local tensional stress was imposed on the joint surface (Bahat, 1991).	688 689 690 691 692 693 694

Figure 10. Standard deviation versus FSR plot of the four main joint sets marked on the left side of the symbols. The saturation level of the FSR ~1.5 is denoted by the vertical black line.	695 696 697
Figure 11. Distribution of joint sets J1 and J2 in the study area. Blue and red arrows mark the J1 (single joint) and J2 (single joint), respectively. The direction (strike) of the arrow represents the average direction obtained for each joint set (see figures 3, 4). The fault and subsurface fault are marked by black and dashed lines, respectively. The change in the regional stress direction (clockwise) from σH_{NW} to σH_{NNW} in the study area is shown in the black dotted frame.	698 699 700 701 702 703
Figure 12. Distribution of joint sets J3 and J4 in the study area. Green and purple arrows mark the J3 (single joint) and J4 (single joint), respectively. The direction of the arrow represents the average direction obtained for each joint set (see figures 3 and 4). Dashed green and purple arrows mark the multilayer joints of J3 and J4, respectively. The change in the local stresses direction (counterclockwise) from σH_{NNE} to σH_{N} in the study area is shown in the black dotted frame.	704 705 706 707 708 709 710 711
7. References	712
Al-Zoubi, A., and U. ten Brink (2001), Salt diapirs in the Dead Sea basin and their relationship to Quaternary extensional tectonics. <i>Marine and Petroleum Geology</i> 18, 779–797.	713 714 715
Avni, Y. 1998. Geological evolution of the central and southern Negev as an indicator of the evolution of the Dead Sea Transform western margin in the late Neogene and Quaternary. Ph.D. thesis, Hebrew University, Jerusalem, 240 pp. (in Hebrew, English abstr.).	716 717 718 719

Avni, Y. 2017. Tectonic setting and physiography setting of the Levant. In: Y. Enzel and O. Bar-Yosef (eds.) Quaternary of the Levant (Environment, Climate change and Humans). PP 3-16. Cambridge University Press.	720 721 722
Avni, Y., Garfunkel, Z., Bartov, Y., Ginat, H. 1994. Pleistocene fault system in the central and southern Negev as an indicator for the tectonic and geomorphological history of the Arava Rift margin. Geological Survey of Israel Current Research. 9: 51-58.	723 724 725
Avni, Y., Bartov, Y., Garfunkel, Z., Ginat H., 2000. Evolution of the Paran drainage basin and its relation to the Plio-Pleistocene history of the Arava Rift western margin, Israel. Israel Journal of Earth-Science 49: 215-238.	726 727 728
Avni, Y., Bartov, Y., Garfunkel, Z and Ginat, H. 2001. The Arava Formation – A Pliocene sequence in the Arava Valley and its western margin, southern Israel. <i>Isr. J. Earth Sci.</i> 50: 101-120.	729 730 731
Avni., Y., Segev, A., Ginat, H., 2012. Oligocene regional denudation of the northern Afar dome: Pre- and syn-breakup stages of the Afro-Arabian plate. GSA Bulletin; v. 124, 1871–1897.	732 733 734
Arlegui, L., SimóAn, J.L., 2001. Geometry and distribution of regional joint sets in non-homogeneous stress field: case study in the Ebro basin (Spain). <i>Journal of Structural Geology</i> 23, 297-313.	735 736 737
Baer, G., Segev., 1996. The state of paleostress along the Milhan Fault , southern Israel, with implications on the sense of fault displacement. Geological Survey of Israel, Current Research 9, 51-58.	738 739 740
Bahat, D., 1979. Theoretical considerations on mechanical parameters of joint surfaces based on studies on ceramics. <i>Geological Magazine</i> 116, 81-166.	741 742
Bahat, D., 1998 (a). On joints and paleostress associated with folds along the Syrian Arc in the Negev. <i>Israel Journal of Earth-Science</i> 48, 29-36.	743 744

Bahat, D., 1988 (b). Early single-layer and late multi-layer joints in the Lower Eocene chalks near Beer Sheva, Israel. <i>Annales Tectonicae</i> II, 3-11.	745
	746
Bahat, D., 1991. Tectono-fractography, Springer-Verlag, Berlin. 354 pp.	747
Bahat, D., 1997. Mechanism of dilatant en echelon crack formation in bedded chalk. <i>Journal of Structural Geology</i> 19, 1375-1392.	748
	749
Bahat, D., 1999a. Single-layer burial joints vs single-layer uplift joints in Eocene chalk from the Beer Sheva syncline in Israel. <i>Journal of Structural Geology</i> 21, 293-303.	750
	751
	752
Bahat D., 1999b. On joints and paleostresses associated with folds along the Syrian Arc in the Negev. <i>Israel Journal Earth-Science</i> , 48: 29-36.	753
	754
Bahat, D., Grossmann, H.N.F., 1988. Regional jointing and paleostress in Eocene chalks around Beer Sheva. <i>Israel Journal Earth-Science</i> 37, 181-191.	755
	756
Bahat, D., Bankwitz, P., Bankwitz, E., Bialik., O., Weinberger, R., 2012. Comparative tectonofractography: fracturing in 19 jointing provinces, experimental results, fracture mechanics considerations and province classification. <i>Z. dt. Ges. Geowiss.</i> , 163/4, p. 345–359.	757
	758
	759
	760
Bai, T., Pollard, D.D., 2000. Fracture spacing in layered rocks: a new explanation based on the stress transition. <i>Journal of Structural Geology</i> 22, 43-57.	761
	762
Bai, T., Maerten, L., Gross, M.R., Aydin, A., 2002. Orthogonal cross joints: do they imply a regional stress rotation? <i>Journal of Structural Geology</i> 24, 77-88.	763
	764
Bankwitz, P. & Bankwitz, E. (1994): Event related jointing in rocks on Bornholm island (Denmark). In: <i>Z. geol. Wiss.</i> , 22 (1/2): 97–114.	765
	766
Bartov, Y., 1994, Geological Photomap of Israel and Adjacent Areas (2nd ed.): Jerusalem, Israel, Israel Geological Survey, scale 1:750,000.	767
	768

Bartov, Y., Steinitz. G., Eyal, M., Eyal, Y., 1980. Sinistral movement along the Gulf of Aqaba-its age and relation to the opening of the Red Sea. <i>Nature</i> 285, 220-222.	769
Becker, A., Gross, M.R., 1996. Mechanical for joint saturation in mechanically layered rocks: an example from southern Israel. <i>Tectonophysics</i> 257, 223-237.	770
Benjamini, C., 1979. Facies Relationship in the Avdat Group (Eocene) in the northern Negev, Israel. <i>Israel Journal of Earth-Science</i> 28, 47-69.	771
Benjamini, C., 1984. Stratigraphy of the Eocene of the Arava Valley (eastern and southern Negev, southern Israel). <i>Israel Journal of Earth-Science</i> 33, 167-177.	772
Ben-Menahem A, Nur A, Vered M (1976) Tectonics, seismicity and structure of the Afro-Eurasian junction - the breaking of an incoherent plate. <i>Phys Earth Planet Inter</i> 12: 1-50	773
Bentor, Y.K., Vroman, A., 1963. The geological map of Israel. Ser. A, The Negev. Sheet 17: Nizana, 100,000. Geological Survey of Israel.	774
Bevan, T.G., Hancock, P.L., 1986. A late Cenozoic regional mesofracture system in southern England and northern France. <i>Journal of Structural Geology</i> 142, 355-362.	775
Braun, M., 1967. Type sections of Avdat group Eocene formations in the Negev, southern Israel. Geological Survey of Israel. <i>Stratigraphic Sections</i> 4:15 p.	776
Calvo, R., and Bartov, Y., 2001, Hazeva Group, southern Israel: New observations and their implications for its stratigraphy, paleogeography and tectono-sedimentary regime: <i>Israel Journal of Earth Sciences</i> , v. 50, p. 71–99.	777
Calvo, R. (2002). Stratigraphy and petrology of the Hazeva Formation in the Arava and the Negev: Implications for the development of sedimentary basins and the morphotectonics of the Dead Sea Rift Valley (in Hebrew, English abstract)	778
Geological Survey of Israel, Report No. GSI/22/2002, 264 p.	779

Chu, H-T., Lee, J-C., Bergerat, F., Hu, J-C., Liang, S-H., Lu, C-Y., Lee, T-Q., 2013.	794
Fracture patterns and their relations to mountain building in a fold-thrust belt: A case study in NW Taiwan. <i>Bull. Soc. géol. France</i> , 184, (4-5), pp. 485-500	795
Cooke, M.L., Underwood, C.A., 2001. Fracrure termination and step-over at bedding interfaces due to frictional slip and interface opening. <i>Journal of Structural Geology</i> 23, 223-238.	797
Dewey, J. F., Holdsworth, R. E., Strachan, R. A., 1998. Transpression and transtension zones. <i>Geological Society London Special Publications</i> 135(1), 1–14.	798
Dunne, W.M., North, C.P., 1990. Orthogonal fracture systems as the limits of thrusting: an example from southwestern Wales. <i>Journal of Structural Geology</i> 12, 207-215.	799
Dyer, R., 1988. Using joint interactions to estimate paleosress ratios. <i>Journal of Structural Geology</i> 10, 685-699.	800
Eldeen, Z.U., Delvaux, D., Jacobs, P., 2000. Tectonic and paleostress evolution in the Wadi Araba segment of the Dead Sea rift, SWJordan. The first Stephan Mueller Conference of European Geophysical Society (EGS). From Continental Breakup to Collision. Israel, Dead Sea. Abstract 103 pp.	801
Engelder, T., 1982. Is there a genetic relationship between selected regional joints and contemporary stress within the lithosphere of North America? <i>Tectonics</i> 1, 161-177.	802
Engelder, T., 1985. Loading path to joint propagation during a tectonic cycle: an example from the Appalachian Plateau, U.S.A. <i>Journal of Structural Geology</i> 7, 459-476.	803
Engelder, T., Geiser, P., 1980. On the use of regional joint sets as trajectories of paleostress fields during the development off Appalachian Plateau, New York. <i>Journal of Geophysical Research</i> 85, 6319-6341.	804

Engelder, T., Lacazette, A., 1990, Natural hydraulic fracturing: p. 35 - 43 in N. Barton and O. Stephansson (editors): Rock Joints: Proceedings of the international symposium on rock joints. Loen, Norway. June 4-6, 1990: A.A. Balkema, Brookfield	818 819 820 821
Engelder, T., Gross, M.R., Pinkerton, P., 1997. Joint development in clastic rocks of the Elk Basin anticline, Montana±Wyoming: an analysis of fracture spacing versus bed thickness in a basement-involved Laramide structure. In: Hoak, T.E., Klawitter, A.L., Blomquist, P.K. (Eds.), Fractured Reservoirs; Characterization and Modeling, Rocky Mountain Association of Geologists, pp. 1±18.	822 823 824 825 826
Eyal, Y., 1996. Stress field fluctuations along the Dead Sea Rift since the Middle Miocene. <i>Tectonics</i> 15, 157-170.	827 828
Eyal, M., Eyal, Y., Bartov, Y., Steinitz, G., 1981. The tectonic development of the western margins of the Gulf of Elat (Aqaba) rift. <i>Tectonophysics</i> 80, 53-66.	829 830
Eyal, Y., Reches, Z., 1983. Tectonic analysis of the Dead Sea Rift region. <i>Tectonics</i> . 2, 167-185.	831 832
Eyal, Y., Gross, M.R., Englder, T., Becker, A., 2001. Joint development during fluctuation of the regional stress field in southern Israel. <i>Journal of Structural Geology</i> 23, 279-298.	833 834 835
Fischer, M.P., 1994. Application of linear elastic fracture mechanics to some problems of fracture propagation in rock and ice. Ph.D. thesis, Pennsylvania State University.	836 837
Flexer, A., Dimant, E., Polishook, B., livnat, A., 1984. Relation of joints in the 'Avedat group (Eocene) to the tectonic pattern of Israel. <i>Israel Journal of Earth-Science</i> 33, 12-25.	838 839 840
Flinn, D., 1977. Transcurrent faults and associated cataclasis in Shetland, <i>J. Geol. Soc.</i> , 133(3), 231– 247, doi:10.1144/gsjgs.133.3.0231.	841 842

Fossen, H., 2010. Structural geology, Cambridge University Press.	843
Freund, R., Zak, I., Garfunkel, Z., 1968. Age and rate of sinistral movement along the Dead Sea Rift. <i>Nature</i> 220, 253-255.	844
Frieslander, U., 2000. The structure of the Dead Sea Transform emphasizing the Arava using new geophysical data. Ph.D. (in Hebrew, English abstract) thesis, The Hebrew University of Jerusalem, 101 pp.	845
Garfunkel, Z., 1981. Internal structure of the Dead Sea Leaky transform in relation to plate Kinematics. <i>Tectonophysics</i> 80, 81-108.	846
Garfunkel, Z., Ben-Avraham, Z., Kagan, E (Eds.), 2014. Dead Sea Transform Fault System: Reviews, Springer, Dordrecht (2014). 359 pp.	849
Gillespie, P.A., Johnston, J.D., Loriga, M.A., McCaffrey, K.J.W., Walsh, J.J., Watterson, J., 1999. Influence of layering on vein systematics in line samples. In: McCaffrey, K.J.W., Lonergan, L., Wilkinson, J.J. (Eds.), <i>Fractures, Fluid Flow and Mineralization</i> . Geological Society Special Publication 155. Geological Society, pp. 35-56.	850
Ginat, H. 1997. Paleogeography and landscape evolution of Nahal Hiyyon and Nahal Zihor basins. Geological Survey of Israel Report GS1II9/97, 206 pp. (in Hebrew, English abstr.).	851
Ginat, H., Avni, Y. 1994. The Arava Conglomerate: a Pliocene valley deposit crossing the Dead Sea Rift. <i>Geological Survey of Israel Current Research</i> . 9: 59-62.	852
Ginat, H., Enzel, Y. and Avni, Y. 1998, Translocation of Plio-Pleistocene drainage systems along the Dead Sea Transform. <i>Tectonophysics</i> , 284: 151-160.	853
Gomez, F., Khawlie, M., Tabet, C., Nasser Darkal, A., Khair, K., Barazangi, M., 2006. Late Cenozoic uplift along the northern Dead Sea transform in Lebanon and Syria, <i>Earth Planet. Science</i> 241, 913–931.	854

Gross, M.R., 1993. The origin and spacing of cross-joints: examples from the Monterey Formation, Santa Barbara coastline, California. <i>Journal of Structural Geology</i> 15, 737-751.	868 869 870
Gross, M.R., Engelder, T., 1991. A case for Neotectonic joints along the Niagara Escarpment. <i>Tectonics</i> 10, 631-641.	871 872
Gross, M.R., Fischer, M.P., Engelder, T., Greenfield., R.J., 1995. Factors controlling joint spacing in interbedded sedimentary rocks: integrating numerical models with field observation from the Monterey Formation, USA. In: Ameen, M.S (Ed) „Fractography: Fracture topography as a tool in fracture mechanics and stress analysis. Geological Society (London) Special Publication 92, 215-233.	873 874 875 876 877
Gross, M.R., Bahat, D., Becker, A., 1997. Relation between jointing and faulting based on fracture-spacing ratios and fault-slip profiles: a new method to estimate strain in layered rocks. <i>Geology</i> 25, 887-890.	878 879 880
Guidi, G., Caputo, R., Scudero, S., 2013. Regional and local stress field orientation inferred from quantitative analyses of extension joints: Case study from southern Italy. <i>Tectonics</i> 32, 239–251.	881 882 883
Hall, J.K., Calvo, R., 2005, Digital shaded relief maps of Israel (1:500,000).	884
Hancock, P.L., 1985. Brittle microtectonics: principles and practice. <i>Journal of Structural Geology</i> 7, 437-457.	885 886
Hancock, P.L., 1991. Determining contemporary stress directions from neotectonic joint systems. <i>Philosophical Transactions of the Royal Society of London A337</i> , 29-40.	887 888
Hancock, P.L., Engelder, T., 1989. Neotectonic joints. <i>Geological Society of America Bulletin</i> 101, 1197-1208.	889 890
Hatzor, Y., Reches, Z., 1990. Structure and paleostress in the Gilboa' region, western margins of the central Dead Sea rift. <i>Tectonophysics</i> 180, 87-100.	891 892

Heidbach, O., Rajabi, M., Cui, X., Fuchs, K., Müller, B., Reinecker, J., Reiter, K., Tingay, M., Wenzel, F., Xie, F., Ziegler, M.O., Zoback, M.L., Zoback, M., 2018. The World Stress Map database release 2016: Crustal stress pattern across scales.	893 894 895 896
Hofstetter, R., Klinger, Y., Amrat, A., Rivera, Q., L., Dorbath, L. 2007. Stress tensor and focal mechanisms along the Dead Sea fault and related structural elements based on seismological data. <i>Tectonophysics</i> 429 (3–4), 165–181.	897 898 899
Holst, T.B., Foote, G.R., 1981. Joint orientation in Devonian rocks in the northern portion of the lower peninsula of Michigan. <i>Geological Society of America Bulletin</i> 92, 85-93.	900 901 902
Hooker, J.N., Laubach, S.E., Marrett, R., 2013. Fracture-aperture sizedfrequency, spatial distribution, and growth processes in strata-bounded and non-strata-bounded fractures, Cambrian Mesón Group, NW Argentina. <i>Journal of Structural Geology</i> 54, 54-71.	903 904 905 906
Hooker, J. N., Katz, R.F., 2015. Vein spacing in extending, layered rock: The effect of synkinematic cementation. <i>American Journal of Science</i> 315, 557–588.	907 908
Huang, Q., Angelier, J., 1989. Fracture spacing and its relation to bed thickness. <i>Geological Magazine</i> 126, 355-362.	909 910
Hurwitz, S., Z. Garfunkel, Y. Ben-Gai, M. Reznikov, Y. Rotstein, and H. Gvirtzman (2002), The tectonic framework of a complex pull-apart basin: Seismic reflection observations in the Sea of Galilee, Dead Sea transform. <i>Tectonophysics</i> 359, 289–306.	911 912 913 914
Issachar, R., Levi, T., Weinberger, R., 2015. Anisotropy of magnetic susceptibility in diamagnetic limestones reveals deflection of the strain field near the Dead Sea Fault, northern Israel. <i>Tectonophysics</i> , 656 (2015) 175–189.	915 916 917

Issachar, R., T. Levi, S. Marco, and R. Weinberger (2018), Separation of diamagnetic and paramagnetic fabrics reveals strain directions in carbonate rocks, <i>J. Geophys. Res. Solid Earth</i> , doi:10.1002/2017JB014823.	918
Jacoby, Y., Weinberger, R., Levi, T., Marco, S., 2014. Clastic dikes in the Dead Sea basin as indicators of local site amplification. <i>Natural Hazards</i> , DOI 10.1007/s11069-014-1392-0.	921
	922
	923
Ji, S., Zhu, Z., Wang, Z., 1998. Relationship between joint spacing and bed thickness in sedimentary rocks: effects of interbed slip. <i>Geology Magazine</i> 135, 637-655.	924
Jiang, L., Qiu, Z., Wang, Q., Guo, Y., Wu, C., Wu, Z., Xue, Z., 2016. Joint development and tectonic stress field evolution in the southeastern Mesozoic Ordos Basin, west part of North China. <i>Journal of Asian Earth Sciences</i> 127, 47-62.	926
	927
	928
Joffe, S., Garfunkel, Z., 1987. Plate kinematics of the circum Red Sea- a re-evolution. <i>Tectonophysics</i> 141, 5-22.	929
	930
Karcz, Z., 1997. The Geology of the north Paran region. <i>Geological Survey of Israel Report GSI/23/97</i> (in Hebrew).	931
	932
Korngreen, D., 1993; The Eocene Regression in the Arava Valley, Southeastern Israel [M.Sc. thesis]: Beer Sheva, Israel, Ben Gurion University of the Negev, 100 p. (In Hebrew, English abstract.).	933
	934
	935
Lacazette, A., Engelder, T., 1992. Fluid-driven cyclic propagation of a joint in the Ithaca Siltstone, Appalachian Basin, New York: p. 297 - 323 In: B. Evans and T.-F. Wong (Eds.): <i>Fault Mechanics and Transport Properties of Rocks; a festschrift in honor of W. F. Brace</i> : Academic Press, San Diego.	936
	937
	938
	939
Laubach, S.E., Mace, R.E., Nance, H.S., 1995. Fault and joint swarms in a normal fault zone. In: Rossmanith, H.-P. (Ed.), <i>Mechanics of Jointed and Faulted Rock</i> . Balkema, Rotterdam, pp. 305-309.	940
	941
	942

Laubach, S.E., Marrett, R.A., Olson, J.E., Scott, A.R., 1998. Characteristics and origins of coal cleat: A review. <i>International Journal of Coal Geology</i> 35, 175–207.	943
Laubach, S.E., Olson, J.E., Gross, M.R., 2009. Mechanical and fracture stratigraphy AAPG Bulletin 93 (no. 11), 1413–1426.	945
Laubach, S.E., Fall, A., Copley, L.K., Marrett, R., Wilkins, S.J., 2016. Fracture porosity creation and persistence in a basement-involved laramide fold, upper cretaceous Frontier Formation, Green river basin, USA. <i>Geological Magazine</i> 153, 887-910.	947
Laubach, S.E., Lamarche, J., Gauthier, B.D.M., Dunne, W.M., Sanderson, D.J., 2018. Spatial arrangement of faults and opening-mode fractures. <i>Journal of Structural Geology</i> 108, 2-15.	950
Le Be'on, M., Klinger, Y., Me' riaux, A.-S., Al-Qaryouti, M.Y., Finkel, R.C., Mayyas, O.T., Tapponnier, P., 2012. Quaternary morphotectonic mapping of the Wadi Araba and implications for the tectonic activity of the southern Dead Sea fault. <i>Tectonics</i> 31, TC5003, http://dx.doi.org/10.1029/2012TC003112 , 2012.	953
Letouzey, J., Trémolières, P., 1980. Paleo-stress fields around the Mediterranean derived from microtectonics. Comparison with plate tectonic data. <i>Rock Mechanics</i> 9, 173-192.	957
Levi, T., Weinberger, R., 2011. Magnetic fabrics of diamagnetic rocks and the strain field associated with the Dead Sea Fault, northern Israel. <i>Journal of Structural Geology</i> 33 (4), 566–578. http://dx.doi.org/10.1016/j.jsg.2011.02.001 .	960
Liotta, D., 1990. La distribuzione dei joints nel bacino di Santa Barbara (Valdarno superiore): indicazioni sulla tectonica neogenica. <i>Boll. Soc. Geol.</i> 109, 437-444.	963
Livnat, A., Flexer, A., 1987. The tectonic style of the southern Arava Rift margins, Israel: alternating stress field in wrench-rifting processes. <i>Tectonophysics</i> 141, 151-168.	965

Longstaffe, F. J., Calvo, R., Ayalon, A., Donaldson, S. (2003). Stable isotope evidence for multiple fluid regimes during carbonate cementation of the Upper Tertiary Hazeva Formation, Dead Sea Graben, southern Israel Journal of Geochemical Exploration, 80:151-170.	967 968 969 970
Lunina, O.V., Mart, Y., Gladkov, A.S., 2005. Fracturing patterns, stress fields and earthquakes in the Southern Dead Sea rift. Journal of Geodynamics 40, 216–234	971 972
Ma, S and Andrews, D.J., 2010. Inelastic off-fault response and three-dimensional dynamics of earthquake rupture on a strike-slip fault, <i>J. Geophys. Res.</i> , 115 (B04304), 1-16.	973 974 975
Mart, Y., Horowitz, A., 1981. The tectonics of the Timna in southern Israel and the evolution of the Dead Sea rift. Tectonophysics 79, 165-199.	976 977
Mart, Y., Ryan, W.B.F., Lunina, O.V., 2005. Review of the tectonics of the Levant Rift system: the structural significance of oblique continental breakup. Tectonophysics 395. 209– 232.	978 979 980
Masson, F., Hamiel Y., Agnon A., Klinger Y., Deprez A., 2015. Variable behavior of the Dead Sea Fault along the southern Arava segment from GPS measurements. Comptes Rendus Geoscience 347, 161–169.	981 982 983
Meirov, T., Hofstetter, A., Kraeva, N., 2007. Measurements of crust displacement and the fault identification in Central Arava (Zofar fault area). GII report, 506/309/07.	984 985
Mitchell, T.M., Faulkner, D.R., 2009. The nature and origin of off-fault damage surrounding strike-slip fault zones with a wide range of displacements: A field study from the Atacama fault system, northern Chile. Journal of Structural Geology 31, 802–816.	986 987 988 989
Narr, W., Suppe, J., 1991. Joint spacing in sedimentary rocks. Journal of Structural Geology 13, 1037-1048.	990 991

Nüchter, J.A., and Ellis, S., 2011, Mid-crustal controls on episodic stress-field rotation around major reverse, normal and strike-slip faults: Geological Society, London, Special Publications, v. 359, no. 1, p. 187–201, doi: 10.1144/SP359.11.	992 993 994
Nuriel, P., G. Rosenbaum, T. I. Uysal, J. Zhao, S. D. Golding, R. Weinberger, V. Karabacak, and Y. Avni (2011), Formation of fault-related calcite precipitates and their implications for dating fault activity in the East Anatolian and Dead Sea fault zones, Geol. Soc. London, Spec. Publ., 359(1), 229–248, doi:10.1144/SP359.13.	995 996 997 998
Nuriel, P., Weinberger, R. Kylander-Clark, A. R.C., Hacker, B., and Craddock, J.P., (2017). The onset of the Dead Sea Transform based on calcite age-strain analyses. Geology, doi:10.1130/G38903.1	999 1000 1001
Odling, N.E., Gillespie, P., Bourgine, B., Castaing, C., Chiles, J.P., Christensen, N.P., Fillion, E., Genter, A., Olsen, C., Thrane, L., Trice, R., Aarseth, E., Walsh, J.J., Watterson, J., 1999. Variations in joint system geometry and their implications for fluid flow in fractured hydrocarbon reservoirs. Petroleum Geoscience 5 (4), 373–384.	1002 1003 1004 1005 1006
Okay, A.I., Demirbağ, E., Kurt, H., Okay, N., Kuşçu, I., 1999. An active deep marine strike-slip basin along the North Anatolian fault in Turkey. Tectonics 18, 29-147.	1007 1008
Palano, M., P. Impressia, and S. Gresta (2013), Current stress and strain-rate fields across the Dead Sea Fault System: Constraints from seismological data and GPS observations, Earth Planet. Sci. Lett., 369–370, 305–316, doi:10.1016/j.epsl.2013.03.043.	1009 1010 1011 1012
Peacock, D.C.P., 2001.The temporal relationship between joints and faults. Journal of Structural Geology 23, 329-341.	1013 1014
Pollard, D.D., Segall, P., Delaney, P.T., 1982. Formation and interpretation of dilatant echelon cracks. Geological Society of America Bulletin 93, 1291-1303.	1015 1016

Pollard, D.D., Aydin, A., 1988. Progress in understanding jointing over the past century.	1017
Geological Society of America Bulletin 100, 1181-1204.	1018
Quennell, A.M., 1959. Tectonics of Dead Sea Rift. Int. Geol. Cong., 20th, Mexico-	1019
Assoc. Serv. Geol. Afr., pp. 385-405.	1020
Rabinovitch, A., Bahat, D., 1999. Model of joint spacing distribution based on shadow	1021
compliance. Journal of Geophysical Research 104, 4877-4886.	1022
Rabinovitch, A., Bahat, D., Melamed, Z., 1999. Technical Note. A note on joint spacing.	1023
Rock Mechanics and Rock Engineering 32, 71-75.	1024
Rabinovitch., Bahat, D., Greenberg, R., 2012. Statistics of joint spacing in rock layers.	1025
Geology Magazine 149 (6), 2012, pp. 1065–1076.	1026
Rawnsley, K.D., T. Rives, J.-P. Petit, S.R. Hencher., Lumsden, A.C., 1992. Joint	1027
development in perturbed stress fields near faults. Journal of Structural	1028
Geology14, 939-951.	1029
Rebai'', S., Philip, H., Taboada, A., 1992. Modern tectonic stress field in the	1030
Mediterranean region: evidence for variation in stress directions at different	1031
scales. Geophysical Journal International 110, 106-140.	1032
Rives, T.,Razack, M., Petit, J-P., Rawnsley, K.D.,1992. Joint spacing: analogue and	1033
numerical simulations. Journal of Structural Geology 14, 925-937.	1034
Ruf, J.C., Rust, K.A., Engelder, T., 1998. Investigation the effect of mechanical	1035
discontinuities on joint spacing. Tectonophysics 295, 245-257.	1036
Sakal, E., 1998, The geology of the Menuha Ridge, Central Negev, Geological Survey of	1037
Israel Report, GSI/14/98 (in Hebrew).	1038
Salamon A, Hofstetter A, Garfunkel Z, Ron H (2003) Seismotectonics of the Sinai	1039
subplate –The eastern Mediterranean region, Geophysical Journal International	1040
155: 149-173.	1041

Sagy, A., Reches, Z., 2006. Joint intensity in layered rocks: The unsaturated, supersaturated, and clustered classes. Israel Journal of Earth Sciences, 1-16.	1042
	1043
Sagy, Y., Gvirtzman, Z., Reshef, M., 2018. 80 m.y. of folding migration: New perspective on the Syrian arc from Levant Basin analysis. Geology 46 (2), 175–178.	1044
	1045
Saucier, F., E. Humphreys, and R. Weldon (1992), Stress near geometrically complex 835 strike-slip faults: Application to the San Andreas Fault at Cajon Pass, southern 836 California, Journal of Geophysical Research, 97(B4), 5081,	1046
	1047
	1048
doi:10.1029/91JB02644.	1049
Schattner, O., Weinberger, R., 2008. A mid-Pleistocene deformation transition in the Hula basin, northern Israel: Implications for the tectonic evolution of the Dead Sea Fault. Geochemistry Geophysics Geosystems 9 (7), 1-18.	1050
	1051
	1052
Simón, J.L., 1989. Late Cenozoic stress field and fracturing in the Iberian Chain and Ebro Basin (Spain). Journal of Structural Geology 11(3), 285-294.	1053
	1054
Sneh, A. 1981. The Hazeva Formation in the northern Arava, Israel. Isr. J. Earth Sci. 30: 81–92.	1055
	1056
Sneh, A., 1996. The Dead Sea Rift: lateral displacement and downfaulting phases. Tectonophysics 263, 277-292.	1057
	1058
Sneh, A., Bartov, Y., Weissbrod, T. and Rosensaft, M., 1998. Geological Map of Israel, 1:200,000. Isr. Geol. Surv. (4 sheets).	1059
	1060
Sneh A, Weinberger R (2014). Major Structures of Israel and Environs, scale 1:500,000. Geological Survey of Israel.	1061
	1062
Tavani, S., Storti, F., Lacombe, O., Corradetti, A., Muñoz, J.A., Mazzoli, S., 2015. Review of deformation pattern templates in foreland basin systems and fold-and-thrust belts: Implications for the state of stress in the frontal regions of thrust wedges. Earth-Science Reviews 141, 82–104.	1063
	1064
	1065
	1066

ten Brink, U., and Z. Ben-Avraham (1989), The anatomy of a pull-apart basin: Seismic reflection observations of the Dead Sea basin, <i>Tectonics</i> 8, 333 – 350.	1067 1068
Trepmann, C., and Stöckhert, B., 2001, Mechanical twinning of jadeite – an indication of synseismic loading beneath the brittle–plastic transition: <i>International Journal of Earth Sciences</i> , v. 90, no. 1, p. 4–13, doi: 10.1007/s005310000165.	1069 1070 1071
Veloso, E.E., Gomila, R., Cembrano, J., González, R., Jensen, E., Arancibia, G., 2015. Stress fields recorded on large-scale strike-slip fault systems: Effects on the tectonic evolution of crustal slivers during oblique subduction. <i>Tectonophysics</i> 664, 244-255.	1072 1073 1074 1075
Voznesensky, V., Sakal, E., Eyal, Y., 2002. Analysis of the joint-sets measured in the Reches Menucha Anticline. Israel Geological Society, Annual Meeting Maagan, Abstract 138 pp.	1076 1077 1078
Weinberger, R., 1999. Initiation and growth of cracks during desiccation of stratified muddy sediments, <i>Journal of Structural Geology</i> , 21:379-386.	1079 1080
Weinberger, R., 2001. Joint nucleation in layered rocks with non-uniform distribution of cavities. <i>Journal of Structural Geology</i> 23, 1241-1254.	1081 1082
Weinberger, R., Bahat, D., 2008. Relative fracture velocities based on fundamental characteristics of joint-surface morphology. <i>Terra Nova</i> 20, 68–73.	1083 1084
Weinberger, R., 2014. Pleistocene Strain Partitioning During Transpression Along the Dead Sea Transform, Metulla Saddle, Northern Israel, in <i>Dead Sea Transform Fault System: Reviews</i> , pp. 151–182, Springer, Dordrecht.	1085 1086 1087
Weinberger, R., Gross, M.R., Sneh, A., 2009. Evolving deformation along a transform plate boundary: Example from the Dead Sea Fault in northern Israel. <i>Tectonics</i> 28, TC5005, 1-19.	1088 1089 1090

Woodworth, J. B., 1896: On the fracture system of joints, with remarks on certain great fractures. In: Proceedings of the Boston Society of Natural History, 27 (9): 163–183.	1091
Wu, H., Pollard, D.D., 1995. An experimental study of relationship between joint spacing and layer thickness. Journal of Structural Geology 17, 887-905.	1092
Yukutake, Y., Iio, Y and Horiuchi, S., 2010. Detailed spatial changes in the stress field of the 1984 western Nagano earthquake region, <i>J. Geophys. Res.</i> , 115 (B6), 1-17.	1093
Zoback, M.D., et al., 1987. New evidence on the state of stress of the San Andreas fault system. Science 238, 1105-1111.	1094
	1095
	1096
	1097
	1098
	1099
	1100

Table 1. The rocks exposed in the study area

Symbol	Lithology	Group	Formation	Age
nql	Conglomerate, silt, lake deposits	Dead Sea	Zhiha	Early Pleistocene
nqc	Conglomerate	Dead Sea	Arava	Pliocene to the Early Pleistocene
m	Conglomerate, sand stone, silt	Tiberius	Hazeva	Miocene
ue	chalky limestone, marl	Avedat	Qzi'ot	Middle to Late Eocene
eav	Limestone, indurated chalk	Avedat	Matred-Paran	Lower-Middle Eocene
enm	Chalk, chalky limestone	Avedat	Paran	Early-Middle Eocene
ea	Chalk with nodular chert layers	Avedat	Mor	Early Eocene
mp	Marl, chalk , Sandy limestone	Mount Scopus	Ghareb - Taqiye	Paleocene – Early Eocene
ca	Chert, Chalk	Mount Scopus	Mishash	Campanian
sc	Chalk, chert, Sandstone	Mount Scopus	Menuha	Coniaciane-Campanian
con	Limestone, dolostone, marl	Judea	Zihor	Coniacian
t	Marl, Limestone, Sandstone	Judea	Ora and Grofit	Turonian
c3	Limestone	Judea	Tamar	Cenomanian
c2	Limestone, dolostone, marl	Judea	En Yorqe'am-Zafir-Avnon Fms.	Cenomanian
c1	dolostone	Judea	Hevyon	Albian-Cenomanian
lck	Sandstone	Kurnub		Lower Cretaceous

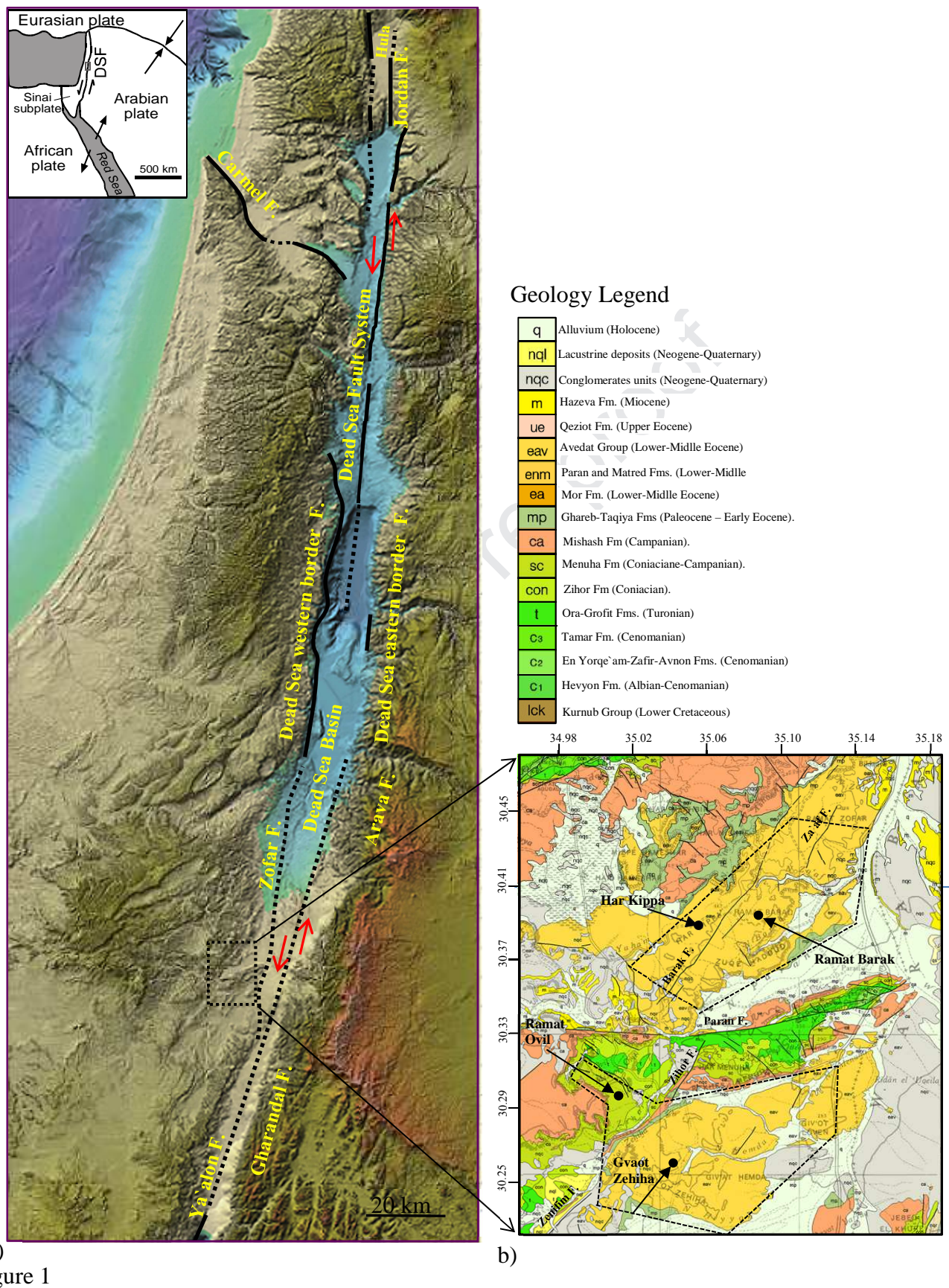


Figure 1

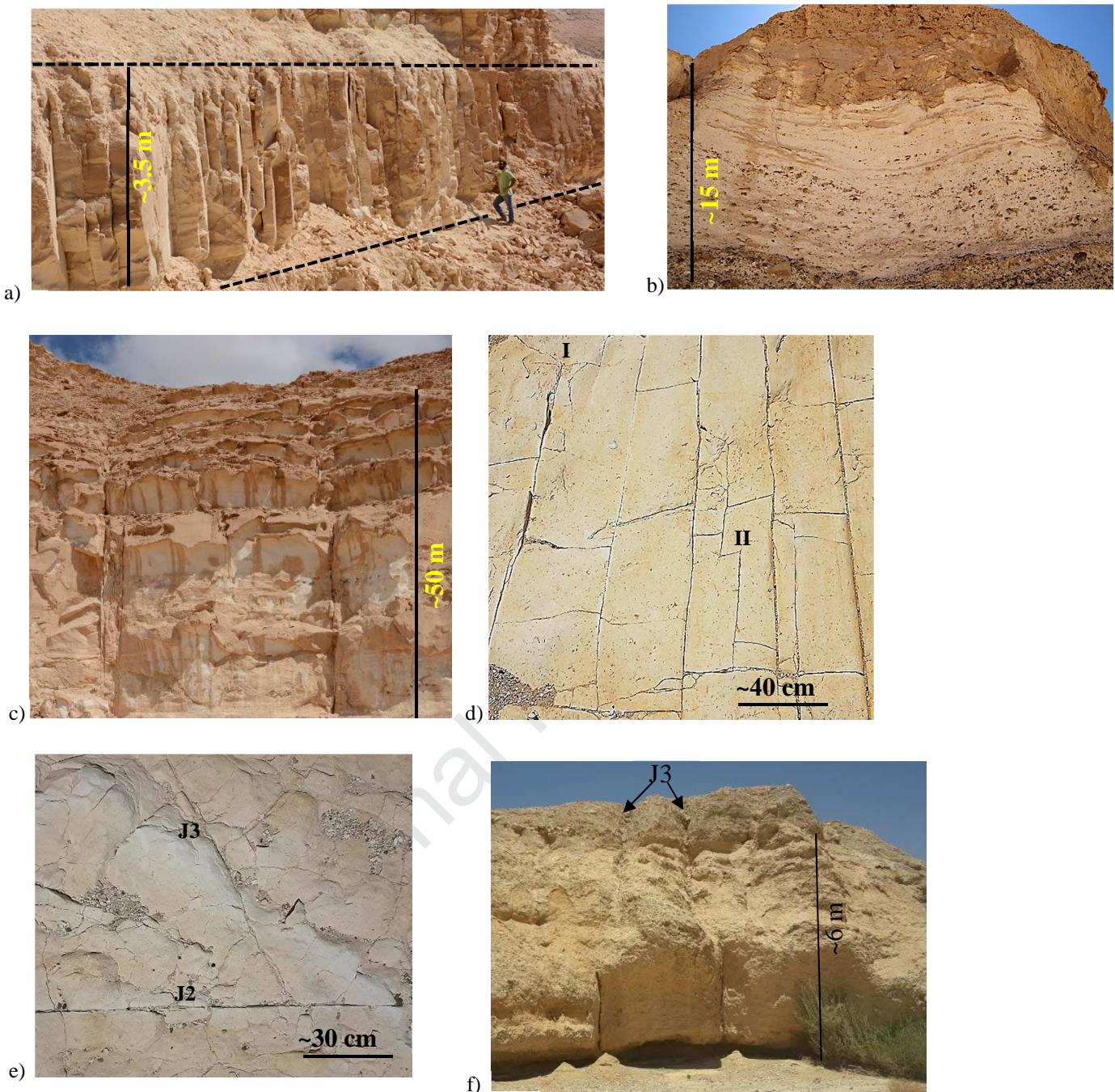


Figure 2

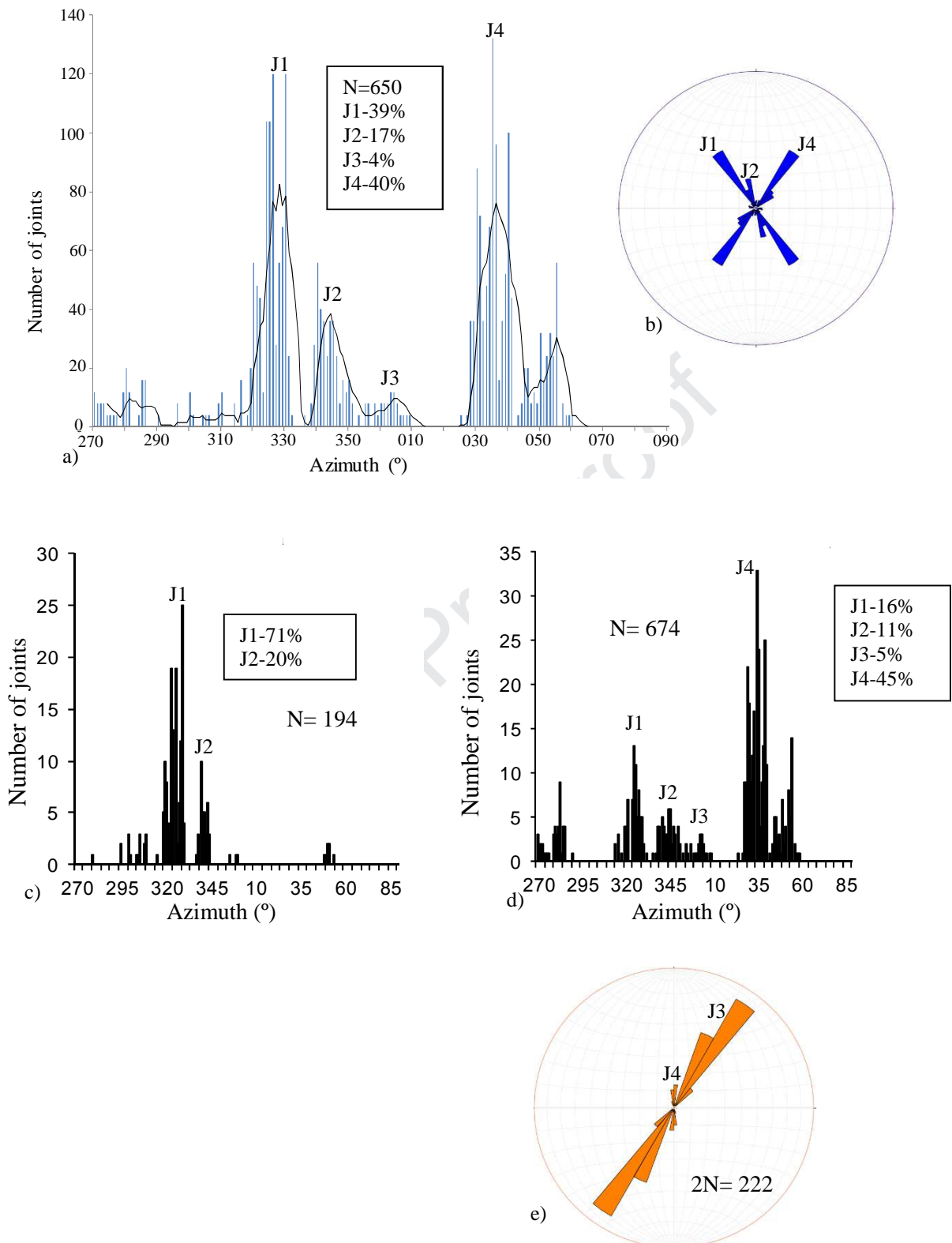


Figure 3.

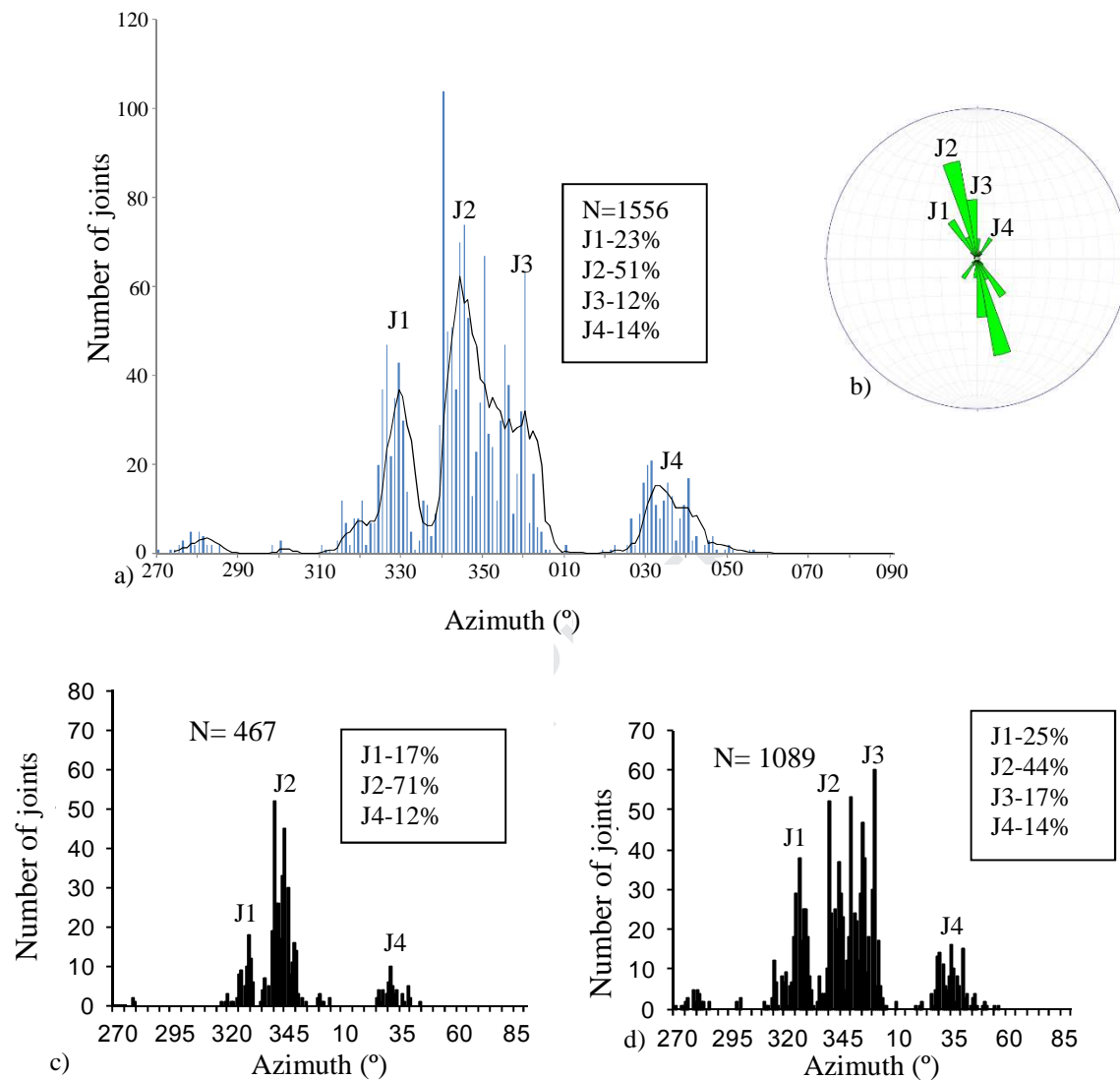


Figure 4.

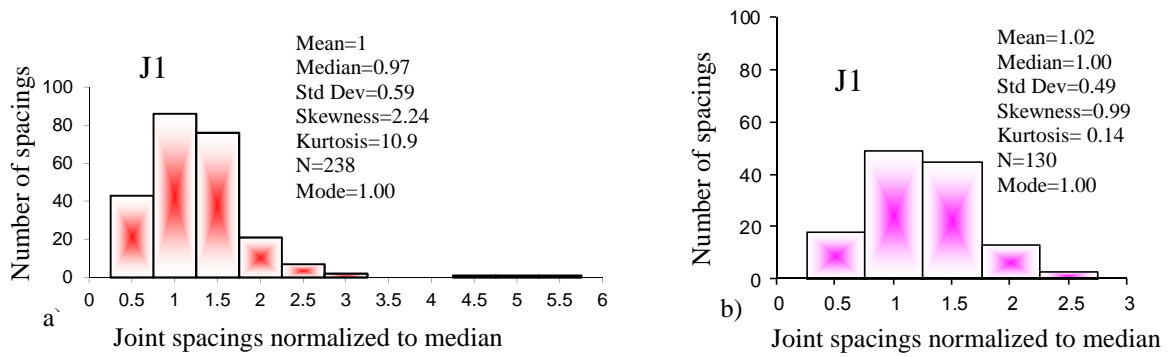


Figure 5.

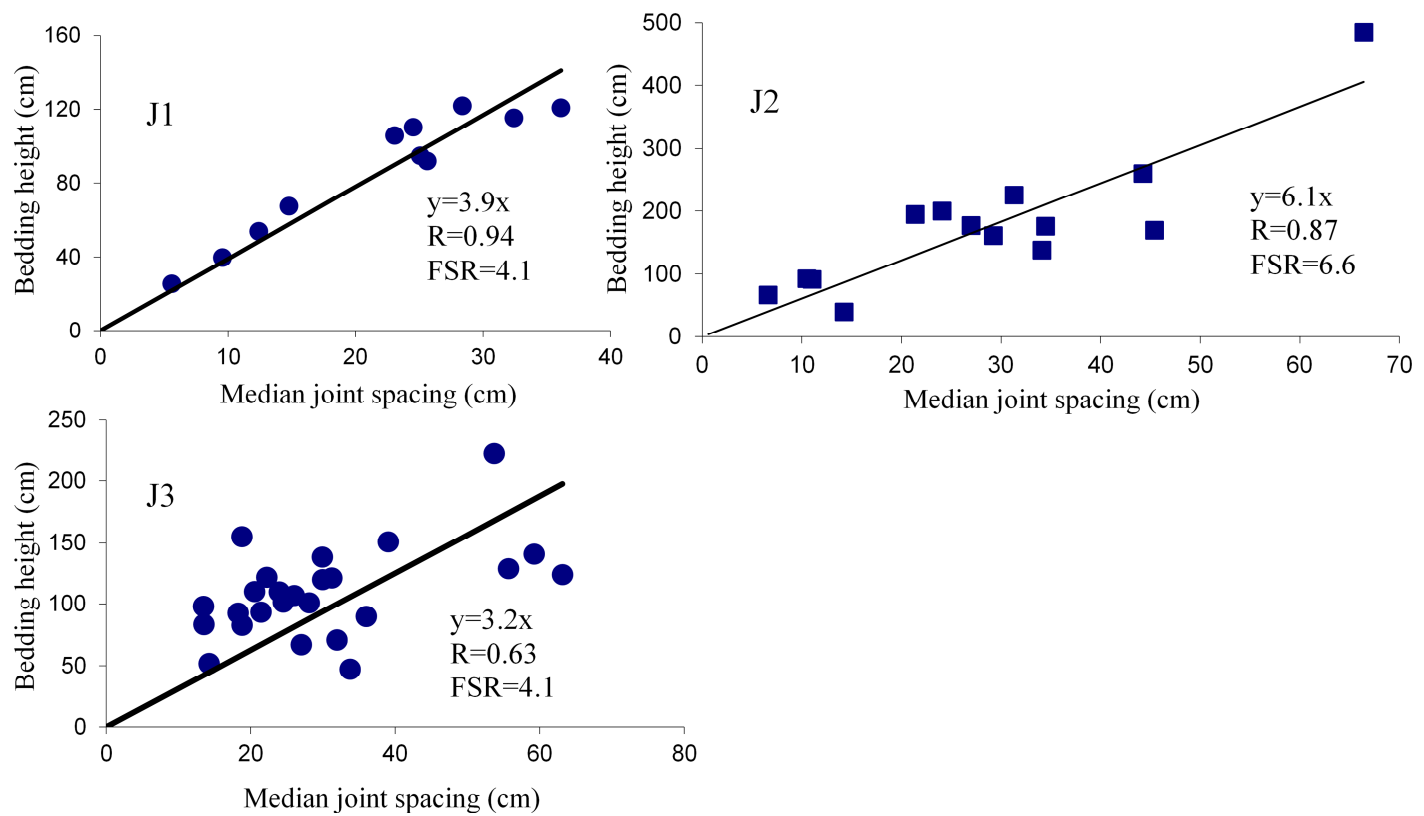
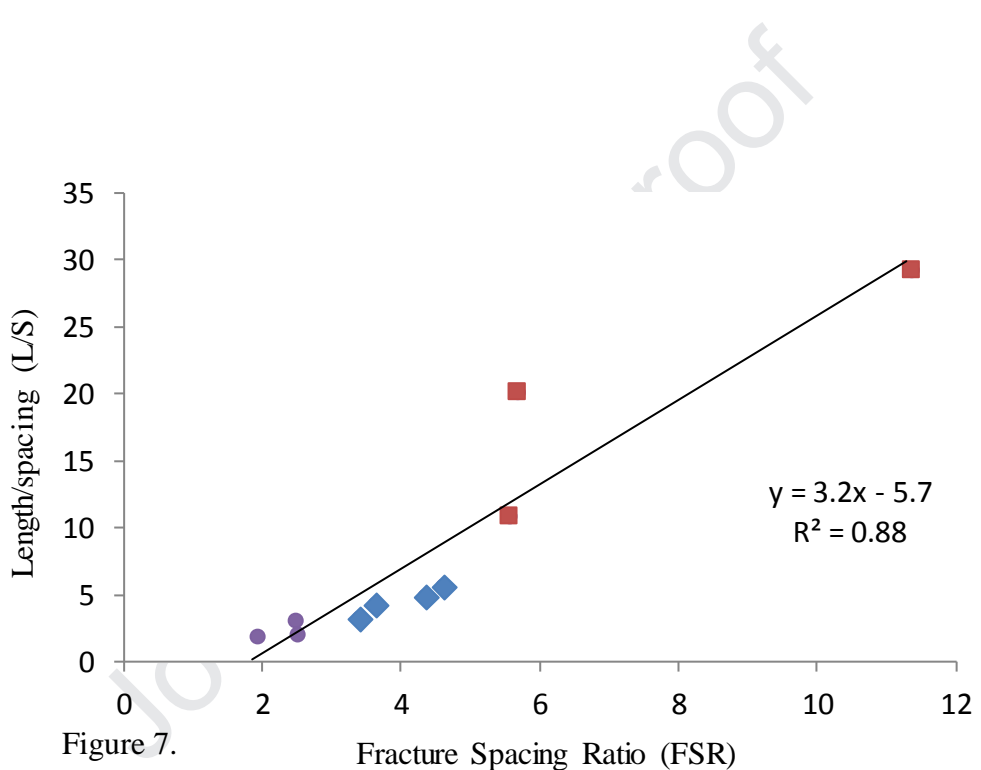


Figure 6



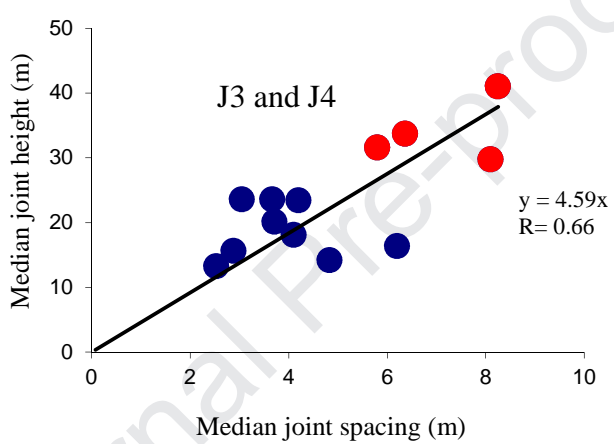


Figure 8.

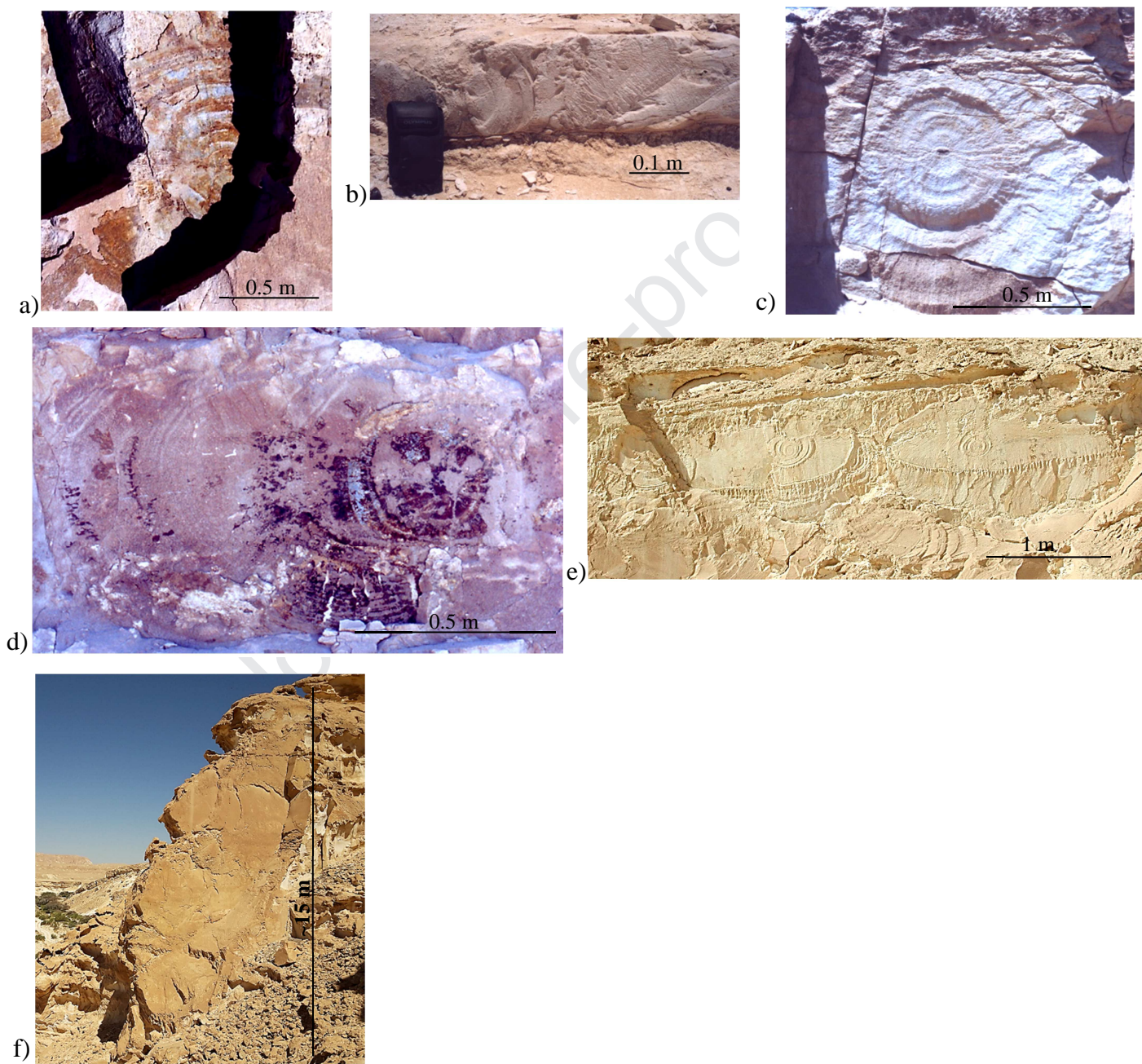
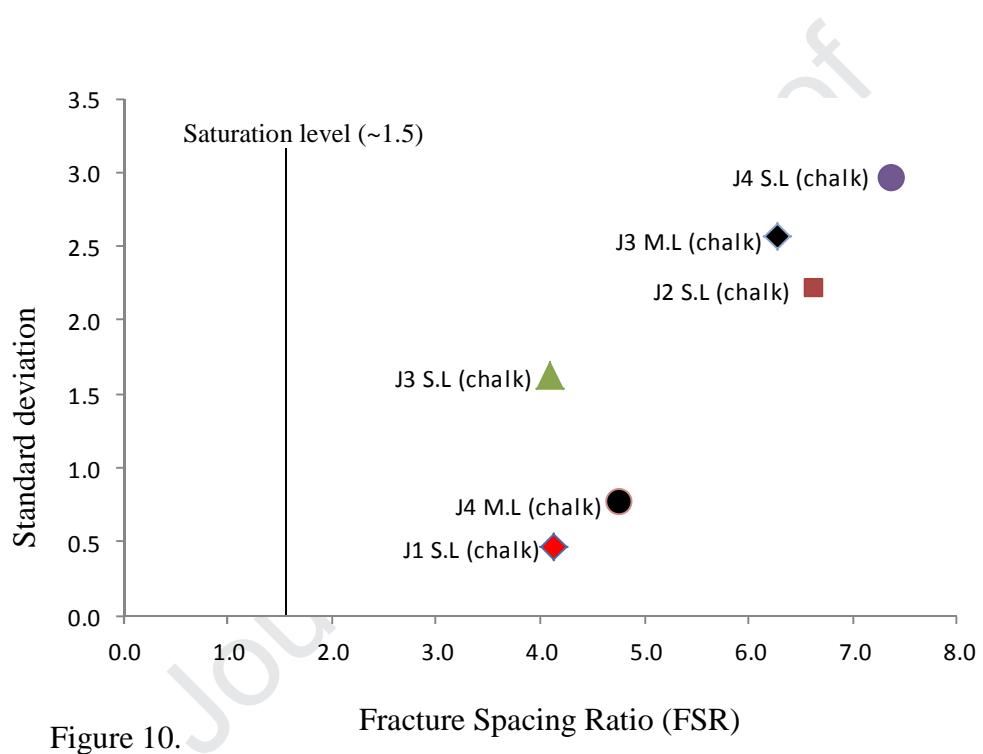


Figure 9.



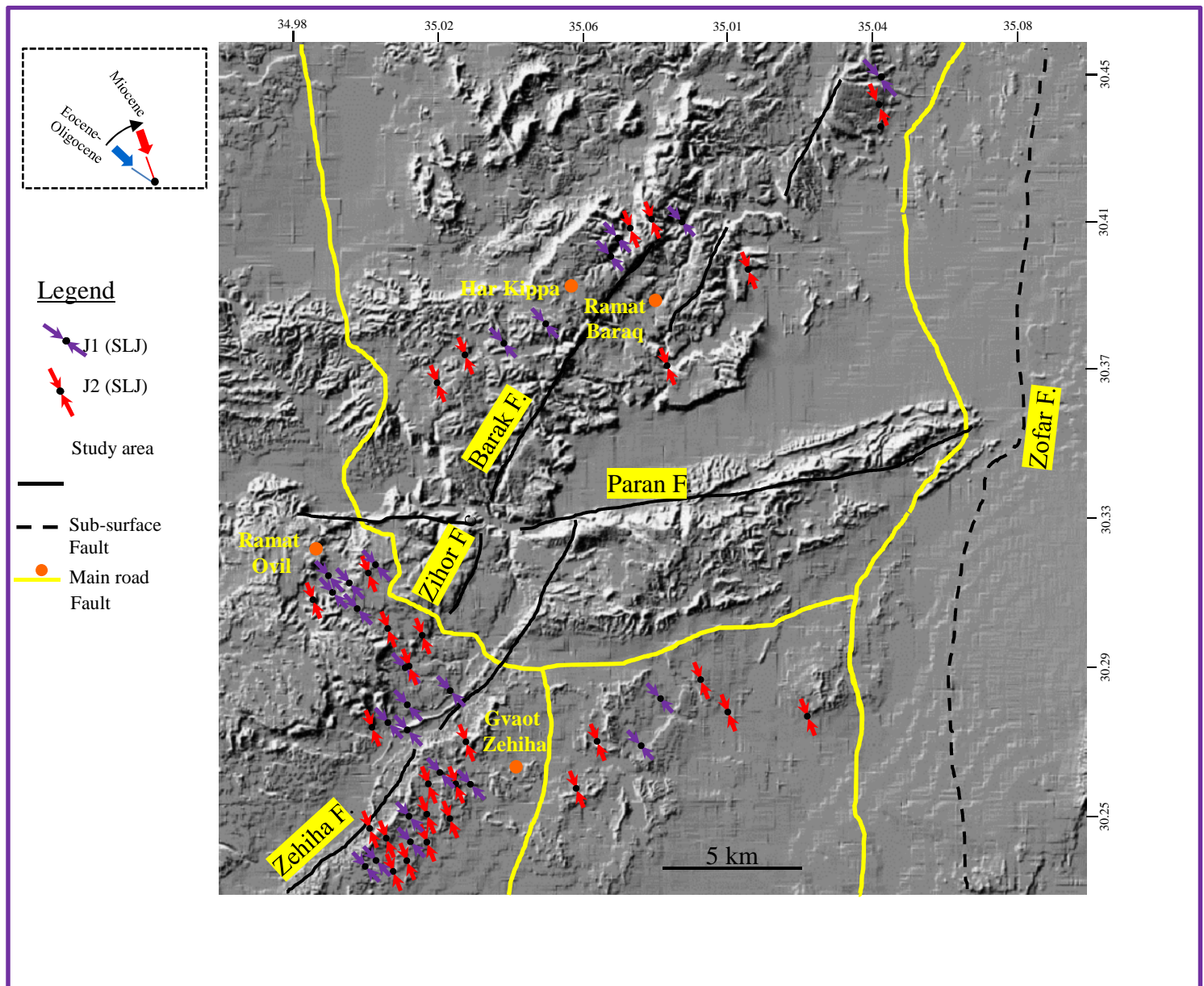


Figure 11.

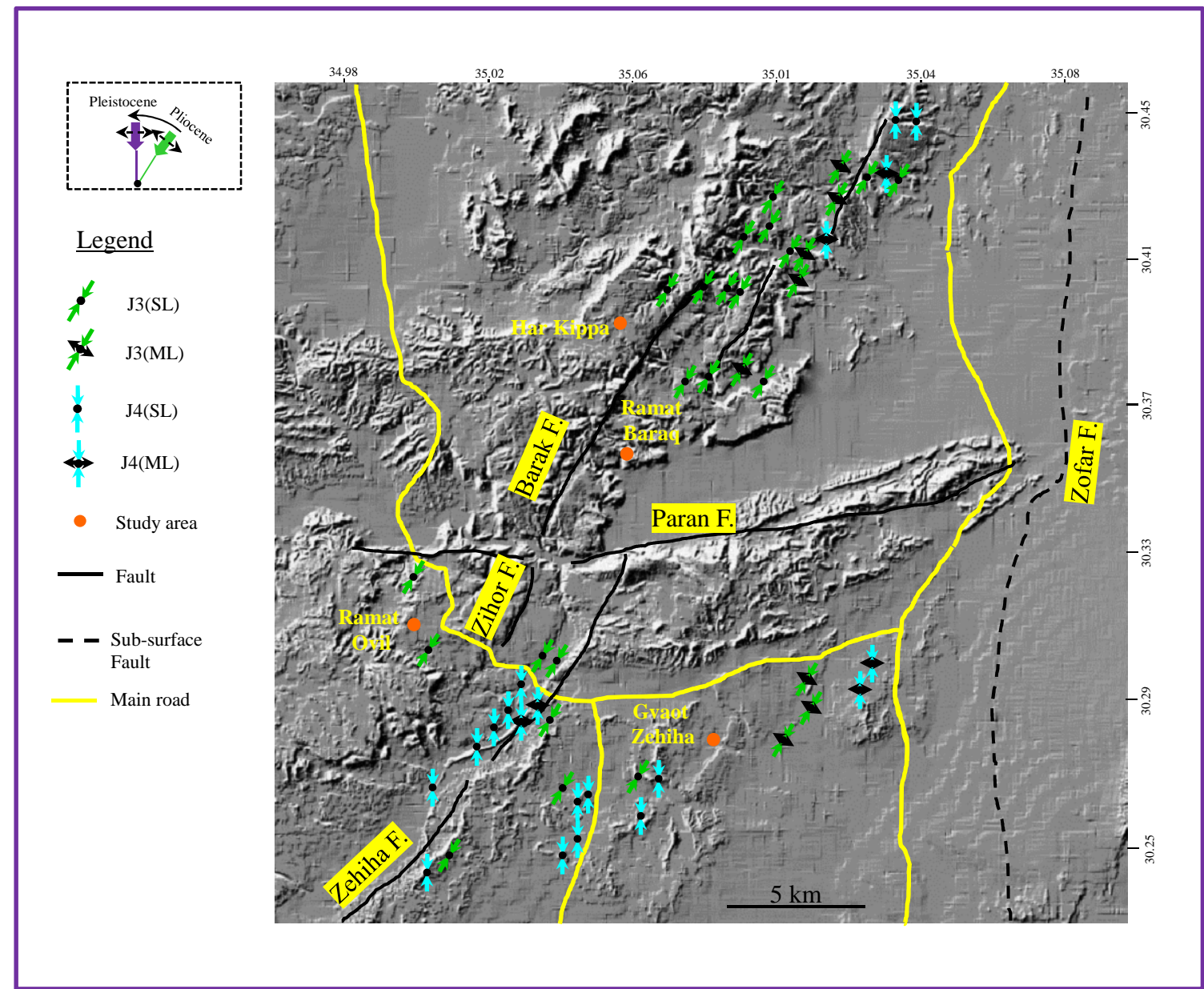


Figure 12.

Research highlights:

- Differences in the joint sets characteristics are related to different tectonic stages, close to the Dead Sea Fault system.
- During the Eocene- Miocene the regional stress field changed from σH_{NW} , to σH_{NNW} , near the Arava Basin
- In the Pliocene-Pleistocene local stress fields, σH_{NNE} and σH_N operated respectively and both were accompanied by a tensional stress field near the Arava Basin